

Iran J Earth Sci., 2026; 18(2): 124-145

Iranian Journal of Earth Sciences (IJES)

https://doi.org/10.57647/j.ijes.2025.16850

Research Article

U–Pb age of the Qobadlu Intrusive body -Evidence for Cretaceous subduction related Magmatism, Northern Sanandaj–Sirjan Zone, NW Iran

Mohammad Najari[1], Ahmad Jahangiri[1]*, Mohsen Moayyed[1], Ryo Anma[2]

[1]*Department of earth and environment sciences, University of Tabriz, Tabriz, Iran*
[2]*Graduate School of Technology, Industrial and Social Sciences, Tokushima University, Minami-Josanjima 2–1, Tokushima 770–8506, Japan*

***Corresponding author:** ahmdj2000@gmail.com

Article History:

Received:
13 January 2024

Revised:
26 October 2024

Accepted:
14 December 2024

Published Online:
25 May 2025

Published in Issue:
30 June 2026

©2026 the Author(s). Published by the OICC Press under the terms of the © CC BY 4.0, Creative Commons Attribution License, which permits use, distribution and reproduction in any medium, provided the original work is properly cited.

Abstract

The Qobadlu intrusive body in the northern part of the Sanandaj – Sirjan Zone (SaSZ) has been recognized as a remnant of Cretaceous magmatic activity in the NW Iran. The Qobadlu gabbroic body has a calc-alkaline affinity. Based on the zircon dating (U-Pb), the coarse grained Qobadlu gabbro were crystallized at 99 Ma. The Low SiO_2 and high Mg # Cr and Ni contents of the Qobadlu rocks can be indicate the upper mantle source for parental magma. Positive anomalies of the LILE and LREE, coupled with negative anomalies of Nb and Ti, and high ratios of La/Nb (1.3-3.3) and Ba/Nb (20-90) can be indicate that the samples are sourced from an amphibole-enriched spinel lherzolitic mantle and developed through Neo-Tethyan subduction regime. Variations in incompatible elements suggest the crustal assimilation and fractionation crystallization during magma ascent. Considering the Cretaceous magmatic activity of the calc-alkaline, these rocks have seemingly formed in the extensional basin related to the Neotethys subduction.

Keyword: Neotethys, Sanandaj–Sirjan Zone, Qobadlu; Spinel lherzolite, U-Pb

Cite this article: Najari, M., Jahangiri, A., Moayyed, M. & Anma, A., (2026). Iranian Journal of Earth Sciences, U–Pb age of the Qobadlu Intrusive body -Evidence for Cretaceous subduction related Magmatism, Northern Sanandaj – Sirjan Zone, NW Iran, 18(2): 124-145.
https://doi.org/10.57647/j.ijes.2025.16850

1. Introduction

Back-arc basins associated with low-K to alkaline magmas with chemical composition controlled by degree of mantle partial melting, assimilation and fractional crystallization (Volpe et al. 1990; Gill 1976; Kent et al. 2002; Pearce and Stern 2006; Stern 2010). The Sanandaj – Sirjan Zone (SaSZ) is about 150 – 250 km-wide and 1500 km-long zone, located immediately to the northeast of the Zagros Thrust zone. It extends SE from the west of the Urumieh Lake in the northwestern Iran, to the Minab Fault in the north of Bandar-Abbas. The initiation of Neo-Tethyan oceanic subduction in the Jurassic is a widely accepted interpretation in the literature on the SaSZ (Berberian and Berberian 1981; Hassanzadeh et al. 2008; Davoudian et al. 2016; Hassanzadeh and Wernicke 2016; Maghdour-Mashhour et al. 2021; Hassanzadeh and Wernicke 2022; Shabanian and Neubauer 2024; Salehpour et al. 2025). However, recent studies have shown enriched mantle contribution in the Jurassic tholeiitic basalts in the northwestern and southeastern parts of the SaSZ (Azizi et al. 2015; Hunziker et al. 2015;

Nazari et al. 2023; Abdolahadi et al. 2025) and suggested that the subduction began in the mid-Cretaceous and that Jurassic magmatism in the SaSZ occurred in a continental rift environment rather than a convergent plate margin above a subduction zone (Hunziker et al. 2015; Azizi and Stern 2019; Shafaii Moghadam et al. 2020) Some researchers further used this localized geochemical evidence to argue that the entire SaSZ formed through the propagation of a continental rift during the Jurassic (Yazdi et al. 2017; Lechmann et al. 2018; Azizi and Stern 2019; Azizi et al. 2020; Lucci et al. 2023; Nouri et al. 2023; Ousta et al. 2024) with subduction initiation occurring in the mid-Cretaceous (Shafaii Moghadam et al. 2020).

Some geologist suggests the mafic bodies in central SaSZ originate arc and back-arc basins source (Arvin et al. 2007). (Azizi et al. 2017) described juvenile granites to the east of Sanandaj and proposed that these rocks originated in an island-arc setting in northern SaSZ. recognized The SaSZ (Fig. 1) is a multi-phase deformed zone that experienced several deformations, metamorphism, and magmatism events throughout its history (Mohajjel et al. 2003), (Hassanzadeh et al. 2008). Metamorphic rocks in this zone include variety of schists, marbles, amphibolite, eclogite, metagranite, and ortho/para-gneiss and meta- sandstones (Davoudian et al. 2008; Malek-Mahmoudi et al. 2017; Dabiri et al. 2018; Kazemi Koohbanani et al. 2018; Mollai et al. 2021; Talebian Borojenie et al., 2025). Several granitoid and gabbroic bodies exist in the SaSZ, with their sizes ranging from small plutonic rocks to batholith bodies extending over an area of 100 km. These intrusive bodies exhibit a NW-SE trend, which is parallel to the trend of structures in Zagros. During the Middle Triassic to Late Jurassic, metamorphosed volcano-sedimentary rocks were exposed in the northern part of the Sanandaj-Sirjan zone (Mohajjel and Fergusson 2000; Mohajjel et al. 2003). These rocks are heterogeneously overlain by Cretaceous limestones (Eftekharnejad 1981; Kazmin et al. 1986; Alavi 1994; Hosseiny 1999; Baharifar et al. 2004; Ashrafi et al. 2024) and exhibit metamorphism ranging from greenschist to amphibolite facies (Eftekharnejad 1981; Mohajjel et al. 2003; Baharifar et al. 2004; KHAN and Ziaei 2007; Davoudian et al. 2008). Studies conducted by Eftekharnejad (1981), Kazmin et al. (1986), Alavi (1994) indicate that the rocks in the northern part of the Sanandaj-Sirjan zone possess calc-alkaline to tholeiitic characteristics and originated from an active continental margin. However, over the past decade, several alternativescenarios have been proposed for this zone, Such as: (1) an immature island arc, (2) a back-arc basin, (3) thinning of the continental lithosphere and/or mantle upwelling, and (4) continental rifting/intraplate activity with mantle plumes (Hosseiny 1999; Azizi and Jahangiri 2008; Mousivand et al. 2011; Nasr-Esfahani 2012; Azizi and Asahara 2013; Ali Rajabzadeh and Esmaeili 2014; Ahmadi Khalaji and Tahmasbi 2015; Azizi et al. 2015; Hunziker et al. 2015; Zarasvandi et al. 2015; Shakerardakani et al. 2021; Nouri et al. 2023). The Qobadlu gabbroic body is located in the southern part of Azarshahr on the eastern margin of Urumieh Lake in the northern part of SaSZ (Fig. 2), where it is extended as a several of outcrops developed along a northwest – southeast trend. Despite the extensive research performed on the SaSZ in the last decade for instance, (Fazlnia 2016) studied the Kharaju mafic pluton and proposed an oblique subduction beneath Central Iran. There are still many ambiguities regarding the magmatic setting, evolution of the SaSZ, and association of the magmatism with the geological evolution in this zone. Accordingly, the present research is an attempt to elucidate for generation of basic mgma with an emphasis on new evidence for new geodynamic model of the northern part of SaSZ. In this study Qobadlu mafic body are investigated based by U–Pb zircon ages, and whole-rock geochemistry data to clarify magma source, magmatic evolution and tectonic setting.

2. Geological setting

According to geochemical and structural evidences (Azizi et al. 2017) the SaSZ has been divided into three parts, as follows:

(1) Northern part, including a series of Cadomian igneous – metamorphic rocks (500 – 600 Ma), Paleozoic granites, and Cretaceous volcano-sediments (Jahangiri 2007; Azizi and Jahangiri 2008; Azizi et al. 2017) which interrupted by Upper Cretaceous to-Paleogene volcanic rocks and granites.

(2) Central part, including (I) Precambrian basement that is composed of amphibolite and meta-granites, and (II) Middle-to-Upper Jurassic high-temperature metamorphic rocks that are formed as interbedding with submarine volcanic rocks. In the central part, granitoid bodies have intruded into Early-to-Middle Jurassic metamorphized volcano-sedimentary complex and exhibit an age of 170 – 140 Ma (Azizi et al. 2011; Azizi et al. 2015). Abundance and distribution of granitoids in the central part of the SaSZ are much higher than other parts of this zone.

(3) Southern part, which is mainly composed of Paleozoic metamorphic rocks, Triassic-Jurassic deposits, and calc-alkaline granites associated with the Neotethys subduction (Arvin et al. 2007; Fazlnia et al. 2009).

The magmatic-sedimentary complex in the south of Azarshahr is including of dark grey shale units and basic/acidic volcanic rocks accompanied by spilitic basalts (Ghadirzadeh and Anvari 1998). This complex comprises the most prominent and extensive Cretaceous

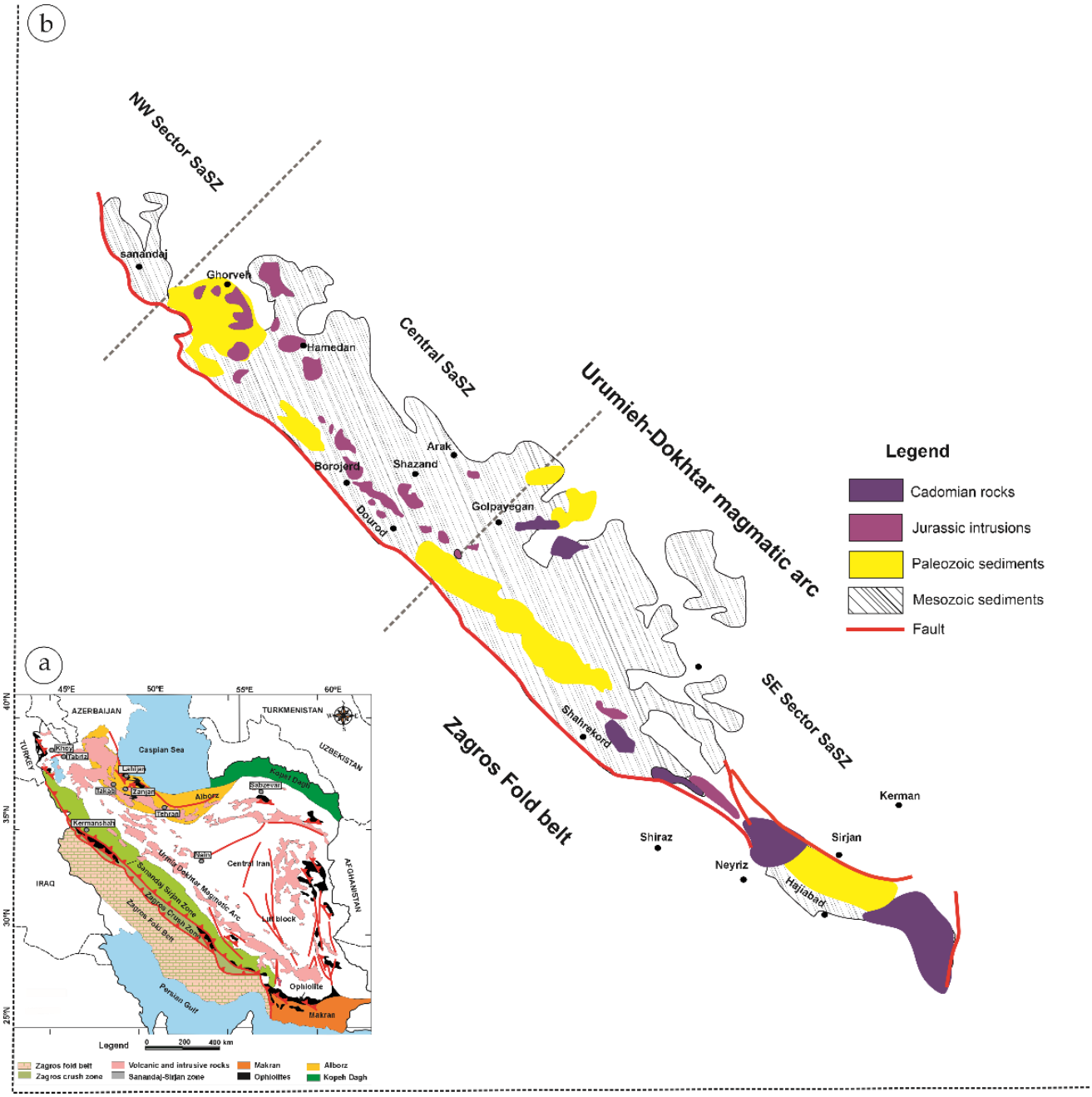


Figure 1. (a) Structural units of Iran Stocklin and Nabavi (1973), (b) Simplified geological map of western Iran modified from (Bayati et al. 2017)

unit in the south and southwest of Azarshahr. The shaly sandstone units in this complex contain macrofossils of a variety of Cretaceous gastropods. The volcanic units of this complex are dominated by rhyolite and the basic lavas are composed of basalt and spilitic basalt, which are sparsely placed within the Cretaceous shaly sandstone units. There are lineated shales along the contact of the basic units, The sedimentary rocks are silicified and affected by low-grade contact metamorphism .These sedimentary rocks exhibit evidences of micro folds and fossils of ammonite, making them dated back to Albian – Cenomanian. These Cretaceous units are cut through by the Qobadlu gabbro intrusive body. According to field observations, this body shows a relatively rough morphology with a black color, being moderate- to coarse-grained (Fig. 3).

3. Methodology

All samples for whole rock geochemistry analysis were crushed using an agate mill. The major element contents of whole rocks were determined by conventional X-ray fluorescence (XRF) in the Zarazma Company (Iran). Heavy mineral fractions including zircon grains were separated from the gabbro samples using conventional heavy liquid and magnetic separation techniques in the Geological Survey and Mineral Exploration of Iran (GSI).

10.57647/j.ijes.2025.16850

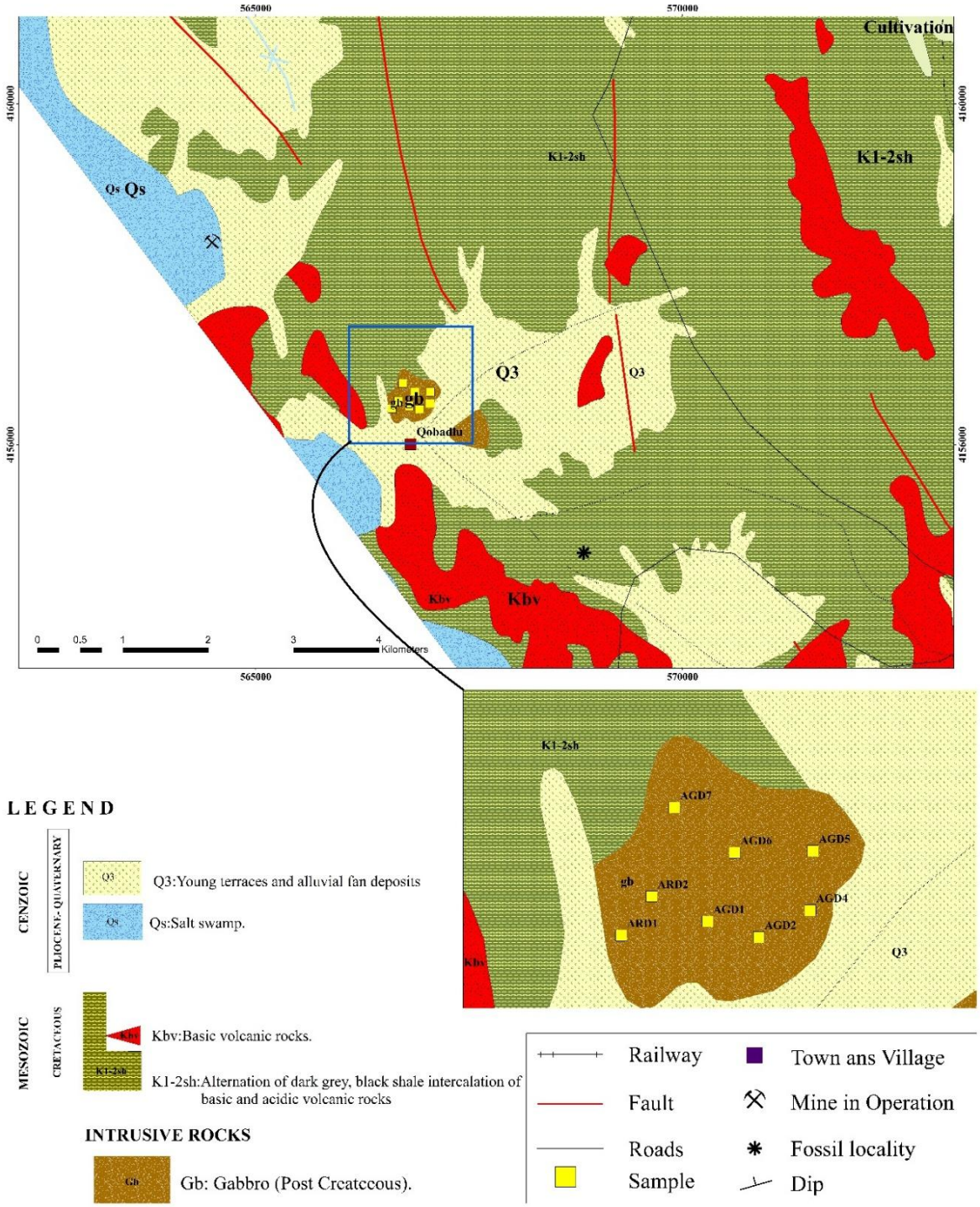


Figure 2. Simplified geological map of Southwestrn of Urmia lake (Alavi-Naini and Shahrabi 1975; Ghadirzadeh and Anvari 1998; Soltani Sisi 2005) Sample location is shown on map

For U-Pb dating, approximately 70 zircon minerals were separated from (Sample AGD-5) the Qobadlu body. Prismatic minerals with no defects or alteration textures/domains and their shooting points for the U-Pb dating were selected based on the BSE and CL observations. U-Pb dating was obtained with a laser ablation (LA, NWR213 Electro Scientific Industries) – mL of 70% $HClO_4$ at 120–140 °C on a hotplate for 3 days until the powder is completely dissolved. After removing inductively coupled plasma mass spectrometer (ICP-MS Agilent 7700x) at Advanced Institute of Science and Technology (AIST), Japan. A detailed description of the LA-ICP-MS analysis is provided in (Kouchi et al. 2015) and (Orihashi et al. 2008). (After Prepare the sample solution by decomposing 100 mg of rock powder in a covered PTFE beaker using 3 mL of 50% HF and 0.5–1 the PTFE cover, dry the dissolved samples at 140 °C on a hotplate with infrared lamps for up to 2 Days.

10.57647/j.ijes.2025.16850

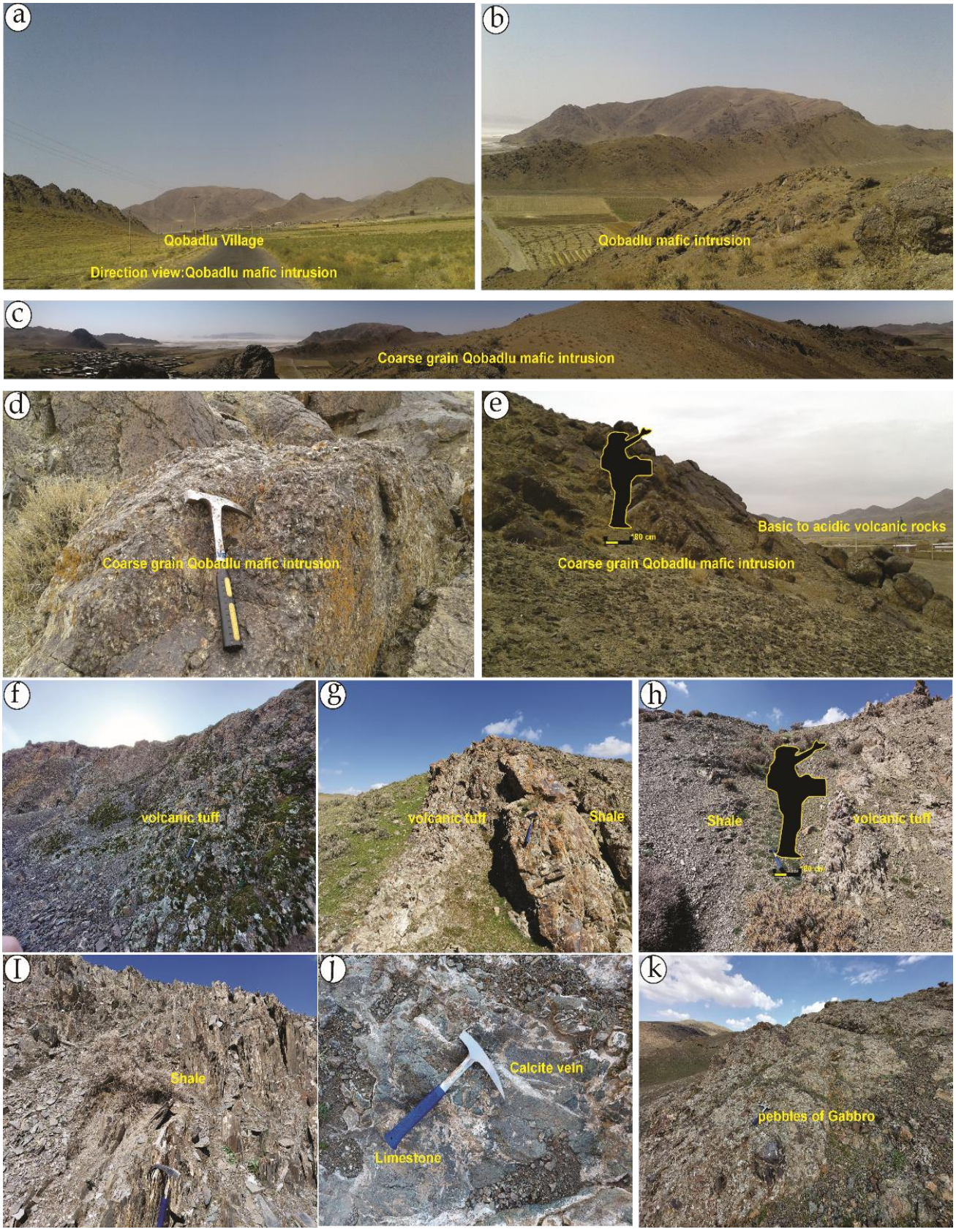


Figure 3. (a-e) Coarse grain Qobadlu mafic intrusive body, (f) tuff, (g) Medium grain sandy sparite and some part sandy microsparite with calcite vein, (h-i) Sequences of Cretaceous shale and interbedded limestone and tuff, (j) interbedded limestone and calcareous shale in the north and northeast of Qobadlu body, (k) pebbles of Gabbro

10.57647/j.ijes.2025.16850

Digest the powdered sample with a mixture of acids (e.g., HNO_3, HF, $HClO_4$, and HCl) in a Teflon beaker or a microwave digestion system to prepare the sample solution. Then calibration standards with known concentrations to establish the calibration curve. Finally, the sample solutions, using the Agilent 7700x ICP-MS instrument and determining the trace element concentrations by comparing their signals with the calibration curve. Which have been thought to be main sources of analytical error in the LA-ICPMS analysis,

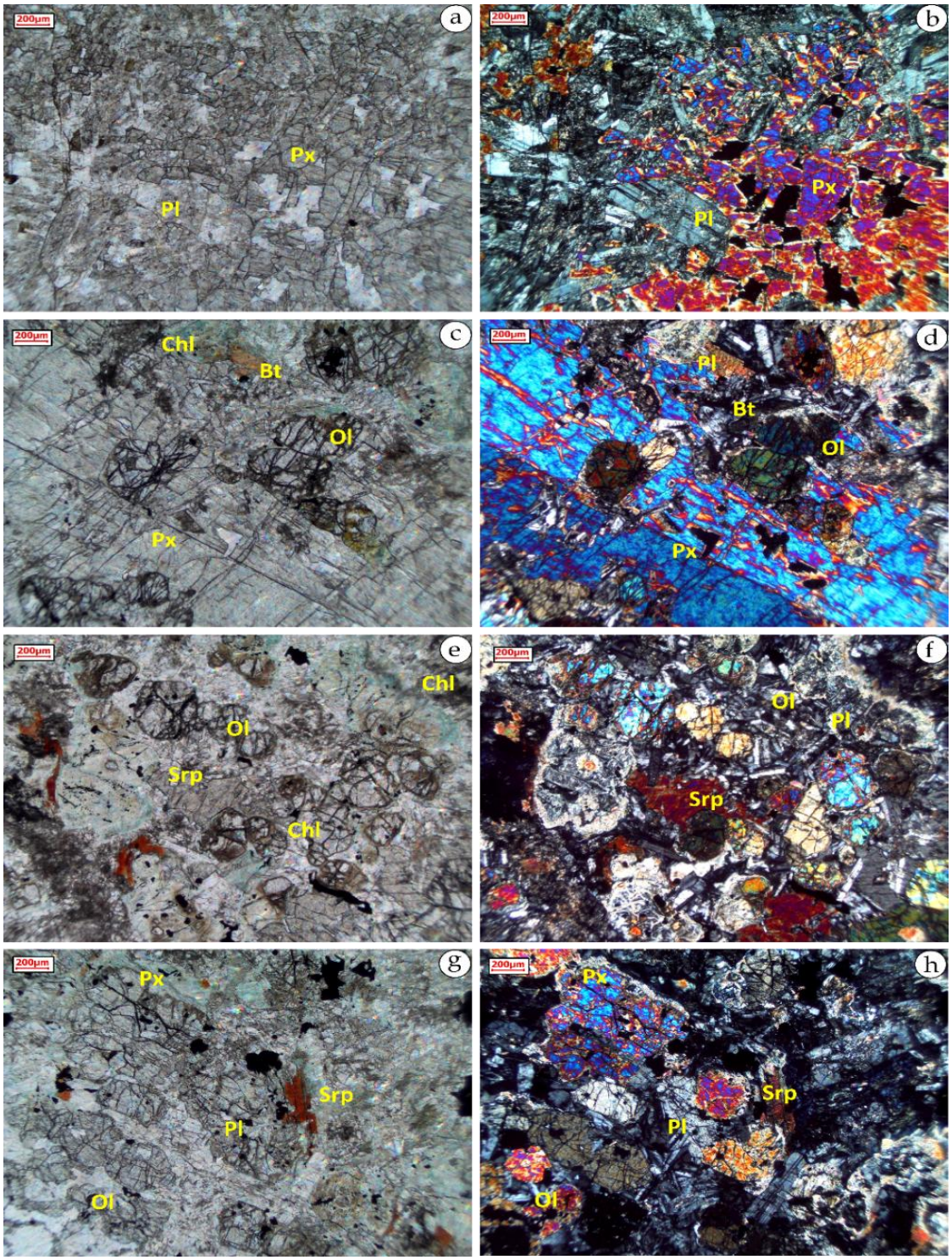


Figure 4. Photomicrographs of the studied igneous rocks. (a,b) Idiomorphic plagioclase. (c,d) photomicrographs showing the major minerals and coarse-grained texture of pyroxene gabbro, Small black grains in clinopyroxene that has orange-red interference color are opaque Fe-Ti oxides (Pl) is the main mineral; clinopyroxene (Cpx) crystallized in spaces between plagioclase grains indicate Intergranular texture.(e-h) clinopyroxene grains are commonly altered to secondary minerals such as magnetite and some grains replaced by biotite (Bt) and Chlorite (Chl) produced by secondary reactions. Abbreviations: Chl = chlorite, Opq = opaque minerals, Pl = plagioclase, Px = pyroxene, Ol= Olivin, Srp= Serpentine. abbreviation from (Whitney and Evans 2010)

10.57647/j.ijes.2025.16850

Table 1. U-Pb isotopic data for zircon crystal determined by LA-ICP-MS

Name	Th/U	$^{207}Pb/^{206}Pb$		Error 2σ	$^{206}Pb/^{238}U$		Error 2σ	$^{207}Pb/^{235}U$		Error 2σ	^{238}U-^{206}Pb age (Ma)		Error 2σ	^{235}U-^{207}Pb age (Ma)		Error 2σ
AG5-01_1	0.97	0.0708	±	0.0047	0.0162	±	0.0006	0.158	±	0.010	114.5	±	5.0	149.0	±	4.5
AG5-01_2	0.98	0.0585	±	0.0041	0.0159	±	0.0006	0.129	±	0.010	110.6	±	4.2	123.5	±	4.3
AG5-02_1	1.15	0.0480	±	0.0027	0.0153	±	0.0006	0.102	±	0.006	98.0	±	2.8	98.2	±	2.8
AG5-02_2	1.07	0.0498	±	0.0025	0.0157	±	0.0006	0.109	±	0.006	99.6	±	3.0	105.1	±	2.8
AG5-03_1	0.99	0.0807	±	0.0048	0.0167	±	0.0006	0.187	±	0.012	134.8	±	4.7	174.2	±	5.1
AG5-03_2	0.86	0.0742	±	0.0046	0.0163	±	0.0006	0.169	±	0.012	128.9	±	5.3	158.9	±	5.0
AG5-05_1	0.98	0.0478	±	0.0037	0.0157	±	0.0006	0.106	±	0.008	101.4	±	3.6	102.2	±	3.8
AG5-06_1	1.50	0.0479	±	0.0021	0.0156	±	0.0006	0.105	±	0.005	101.4	±	2.6	101.3	±	2.5
AG5-06_2	1.06	0.0710	±	0.0042	0.0161	±	0.0007	0.162	±	0.011	115.5	±	4.3	152.1	±	4.6
AG5-06_3	1.11	0.0480	±	0.0029	0.0154	±	0.0006	0.104	±	0.007	99.6	±	3.0	100.4	±	3.3
AG5-07_1	1.04	0.0550	±	0.0033	0.0158	±	0.0007	0.122	±	0.008	103.9	±	3.1	117.1	±	3.6
AG5-07_2	0.96	0.0649	±	0.0054	0.0157	±	0.0007	0.143	±	0.013	114.0	±	4.0	135.9	±	5.6
AG5-08_1	1.06	0.0508	±	0.0031	0.0156	±	0.0007	0.111	±	0.007	99.0	±	3.2	107.0	±	3.3
AG5-08_2	1.09	0.0601	±	0.0035	0.0159	±	0.0007	0.133	±	0.008	109.6	±	3.3	126.9	±	3.6
AG5-08_3	1.07	0.0585	±	0.0032	0.0154	±	0.0006	0.127	±	0.007	109.6	±	3.4	121.0	±	3.3
AG5-08_4	1.03	0.0474	±	0.0030	0.0155	±	0.0006	0.104	±	0.007	100.9	±	3.2	100.7	±	3.3
AG5-09_1	1.00	0.0482	±	0.0034	0.0158	±	0.0006	0.108	±	0.008	100.3	±	3.3	103.9	±	3.8
AG5-09_2	1.04	0.0539	±	0.0038	0.0158	±	0.0007	0.119	±	0.009	105.4	±	3.8	113.9	±	4.0
AG5-10_1	1.71	0.1496	±	0.0045	0.0178	±	0.0007	0.375	±	0.016	151.6	±	3.9	323.4	±	5.9
AG5-10_2	1.24	0.0677	±	0.0028	0.0158	±	0.0007	0.150	±	0.007	113.1	±	3.0	141.8	±	3.1
AG5-10_3	1.35	0.0638	±	0.0032	0.0158	±	0.0007	0.142	±	0.007	108.9	±	2.9	134.4	±	3.3
AG5-10_4	1.21	0.0605	±	0.0021	0.0159	±	0.0006	0.135	±	0.006	107.2	±	2.7	128.9	±	2.7
AG5-11_1	1.36	0.0471	±	0.0036	0.0153	±	0.0006	0.100	±	0.008	100.1	±	3.2	97.1	±	3.7
AG5-11_2	1.32	0.0499	±	0.0026	0.0154	±	0.0006	0.108	±	0.006	98.7	±	2.7	104.5	±	2.9
AG5-11_3	1.17	0.0516	±	0.0028	0.0154	±	0.0006	0.113	±	0.007	97.3	±	2.9	108.3	±	3.1
AG5-12_1	1.49	0.0519	±	0.0027	0.0155	±	0.0006	0.112	±	0.006	102.5	±	2.5	107.9	±	2.8
AG5-12_2	1.63	0.0581	±	0.0025	0.0156	±	0.0006	0.126	±	0.006	102.9	±	2.5	120.5	±	2.8
AG5-12_3	1.62	0.0530	±	0.0024	0.0152	±	0.0006	0.114	±	0.006	101.5	±	2.7	109.5	±	2.7
AG5-13_1	1.04	0.0499	±	0.0039	0.0156	±	0.0007	0.109	±	0.009	103.0	±	3.3	105.3	±	4.0

10.57647/j.ijes.2025.16850

Table 1. U-Pb isotopic data for zircon crystal determined by LA-ICP-MS (Continued)

Name	Th/U	$^{207}Pb/^{206}Pb$		Error 2σ	$^{206}Pb/^{238}U$		Error 2σ	$^{207}Pb/^{235}U$		Error 2σ	^{238}U-^{206}Pb age (Ma)		Error 2σ	^{235}U-^{207}Pb age (Ma)		Error 2σ
AG5-13_2	1.00	0.0575	±	0.0036	0.0154	±	0.0007	0.125	±	0.009	101.8	±	3.2	119.6	±	3.9
AG5-14_1	0.92	0.0504	±	0.0037	0.0160	±	0.0007	0.113	±	0.008	104.1	±	4.1	108.4	±	3.8
AG5-14_2	1.86	0.0515	±	0.0025	0.0154	±	0.0006	0.112	±	0.006	99.5	±	2.3	107.6	±	2.8
AG5-14_3	1.48	0.0521	±	0.0027	0.0154	±	0.0006	0.114	±	0.007	100.2	±	2.6	109.5	±	3.0
AG5-15_1	1.06	0.0473	±	0.0025	0.0158	±	0.0006	0.105	±	0.006	104.0	±	3.0	101.3	±	2.9
AG5-16_1	1.49	0.0484	±	0.0019	0.0156	±	0.0006	0.107	±	0.005	102.2	±	2.4	103.3	±	2.3
AG5-16_2	1.10	0.0521	±	0.0027	0.0154	±	0.0006	0.112	±	0.007	100.0	±	2.8	108.0	±	3.0
AG5-16_3	1.13	0.0461	±	0.0024	0.0155	±	0.0006	0.101	±	0.006	101.1	±	2.9	97.3	±	2.7
AG5-17_1	1.03	0.0526	±	0.0034	0.0154	±	0.0006	0.114	±	0.008	101.2	±	3.4	109.3	±	3.6
AG5-17_2	0.95	0.0516	±	0.0036	0.0150	±	0.0006	0.106	±	0.007	101.7	±	3.7	102.2	±	3.2
AG5-17_3	0.97	0.0523	±	0.0034	0.0155	±	0.0006	0.113	±	0.008	99.6	±	3.4	108.8	±	3.5
AG5-17_4	1.11	0.0493	±	0.0022	0.0155	±	0.0006	0.107	±	0.006	104.0	±	2.6	103.1	±	2.6
AG5-21_1	0.97	0.0576	±	0.0057	0.0158	±	0.0006	0.126	±	0.013	102.8	±	4.8	120.7	±	5.6
AG5-21_2	0.92	0.0635	±	0.0048	0.0161	±	0.0006	0.142	±	0.011	108.7	±	4.6	134.7	±	4.8
AG5-21_3	0.93	0.0499	±	0.0049	0.0155	±	0.0006	0.107	±	0.010	105.9	±	4.4	102.9	±	4.8
AG5-21_4	0.99	0.0797	±	0.0056	0.0163	±	0.0006	0.181	±	0.013	133.5	±	5.1	168.7	±	5.6
AG5-22_1	1.21	0.0535	±	0.0024	0.0156	±	0.0006	0.117	±	0.006	103.0	±	2.6	112.3	±	2.6
AG5-22_2	0.98	0.0569	±	0.0032	0.0158	±	0.0005	0.127	±	0.009	112.8	±	3.4	121.4	±	3.9
AG5-22_3	1.22	0.0516	±	0.0024	0.0154	±	0.0005	0.112	±	0.006	99.2	±	2.4	107.8	±	2.6
AG5-22_4	1.29	0.0510	±	0.0023	0.0158	±	0.0006	0.113	±	0.006	103.5	±	2.7	109.1	±	2.7
AG5-23_1	1.52	0.0496	±	0.0018	0.0157	±	0.0006	0.110	±	0.005	102.2	±	2.6	106.4	±	2.4
AG5-23_2	1.22	0.0526	±	0.0030	0.0158	±	0.0006	0.118	±	0.007	103.9	±	2.6	112.9	±	3.2
AG5-23_3	1.22	0.0470	±	0.0023	0.0153	±	0.0006	0.102	±	0.006	100.7	±	2.8	98.9	±	2.7

Data used for age calculation. * Percentage of ^{206}Pb contributed by common Pb on the basis of ^{204}Pb. Value of common Pb was assumed by (Stacey and Kramers 1975) model.

were measured on a Harvard 91500 zircon crystal) The ISOPLOT v.4.15 program (Ludwig, 2012) was used for calculations of the Concordia and ages, statistics, and isotopic diagram plots.

4. Petrography

The Qobadlu rocks have coarse-grained textures. These rocks mainly dominated by clinopyroxene, biotite, olivine, and plagioclase (Fig. 4a). The most abundant mineral in these rocks is the plagioclase and their average grain size varying from 0.2 to 2.5 mm.

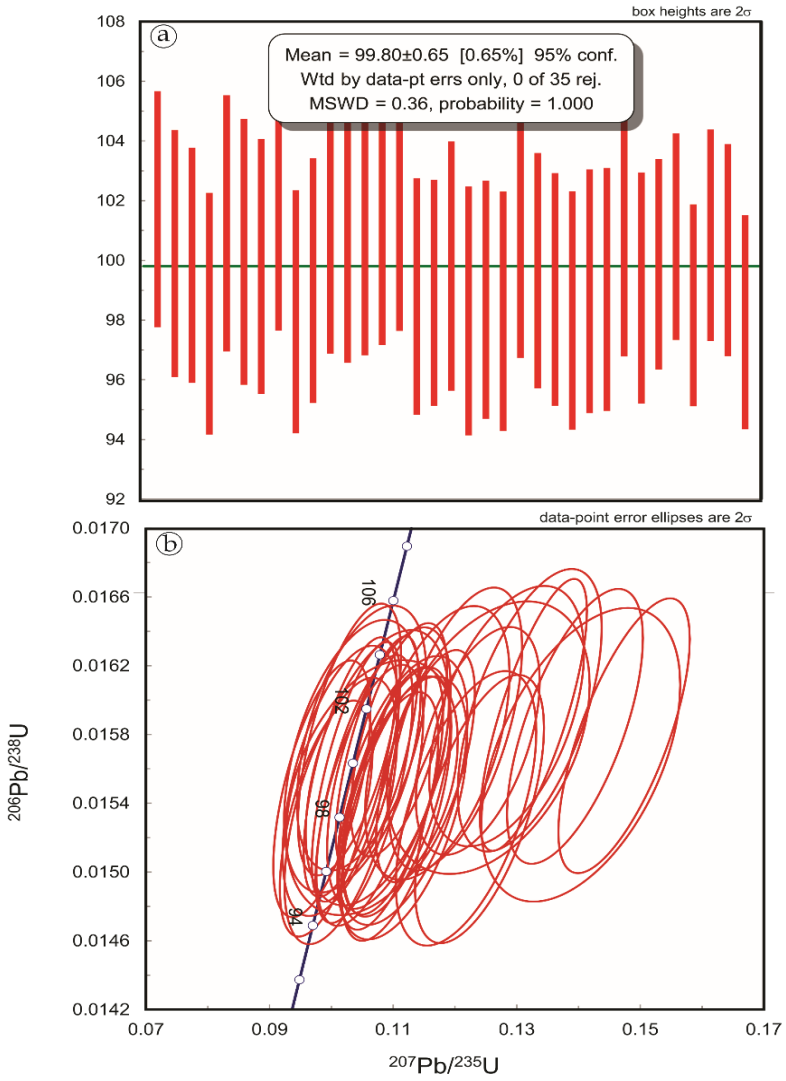


Figure 5. (a) U–Pb Concordia plot of zircon (b) weighted mean $^{206}Pb/^{238}U$ diagram from of AGD-5 sample

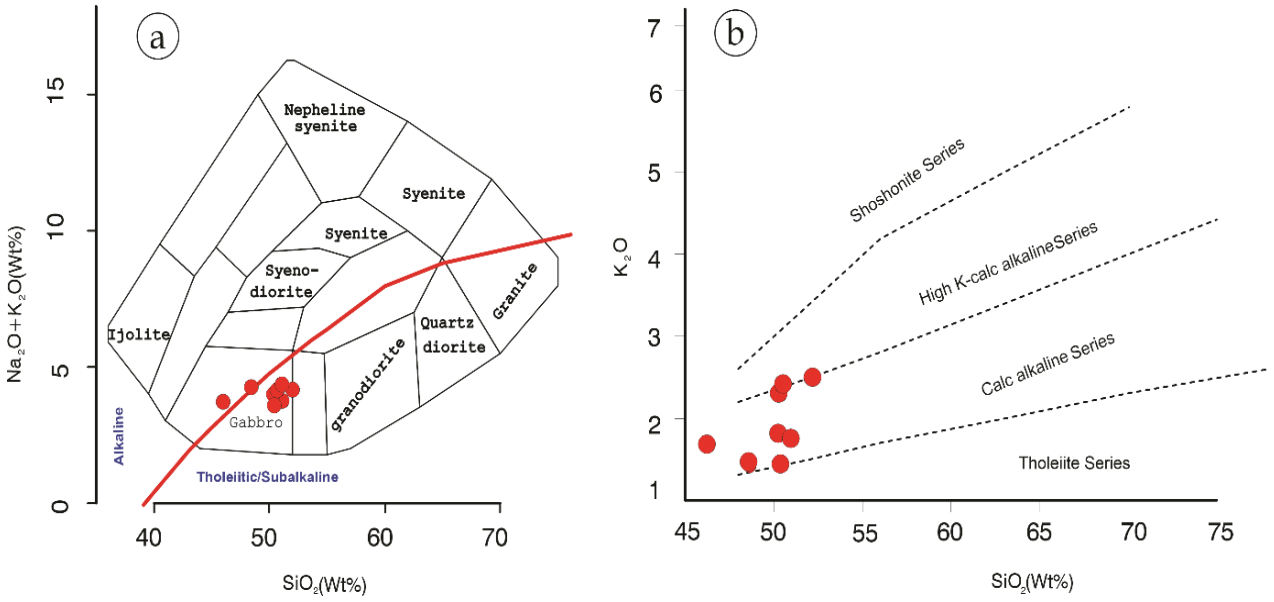


Figure 6. The distributions of mafic rocks in diagrams. (a) Total alkalis versus SiO_2 diagram (Cox et al. 1979), (b) in the K_2O versus SiO_2 variation diagram Peccerillo and Taylor (1976) most samples have Gabbro affinity and plot in calc-alkaline series fields

10.57647/j.ijes.2025.16850

The amount of plagioclase varies from 50% to 70% in different samples. The studied samples display ophitic, intergranular and granular textures (Fig. 4c). Plagioclase minerals are euhedral and display polysynthetic twinning and mostly affected by saussuritization and, less frequently, calcification. The plagioclase grains are commonly surrounded by clinopyroxene. clinopyroxene fills spaces between the plagioclase grains, and the plagioclase was likely crystallized before the clinopyroxene. clinopyroxene grains are distinguished by two directions of cleavage at approximately 87 and 93º, clinopyroxenes are re- placed by hornblende and chlorite, commonly altered and replaced with secondary minerals such as tremolite, actinolite (uralite) and magnetite. Some grains are replaced by amphibole and biotite (Fig. 4e-g).

5. Zircon U-Pb geochronology

One fresh sample, AGD-5 (gabbro) was selected for zircon dating. BSE figures of the Zircon grains are shown in (Fig. 5), images of AGD-5 sample reveal that the zircons are colorless to light gray and euhedral to subhedral where transparent Zircon grains are 80 – 200 microns in length and exhibit prism-like shapes and internal alteration textures. Zircon U-Pb isotope ratios are listed in (Table 1).

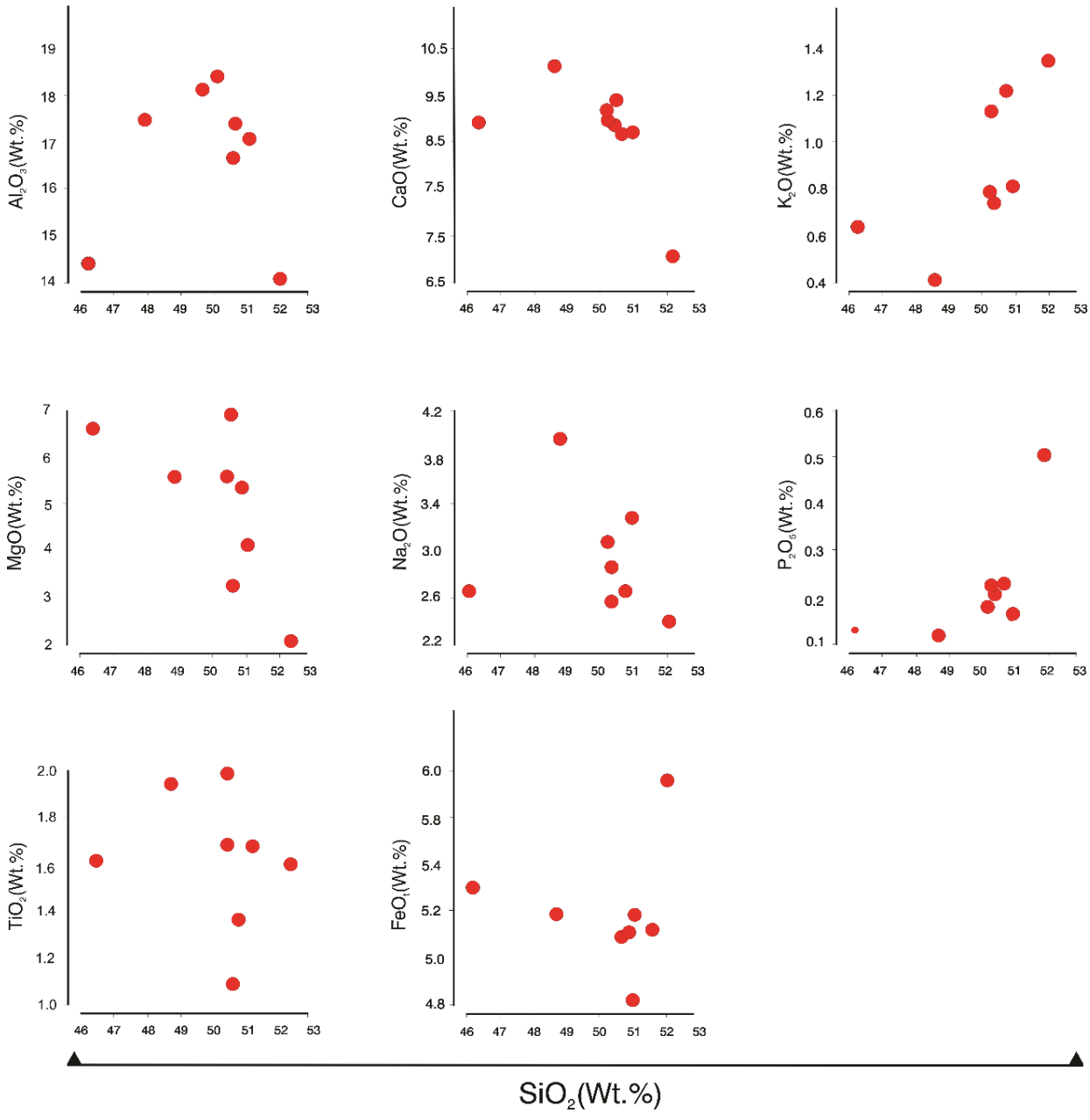


Figure 7. Selected binary diagrams showing major and trace elements variation Qobadlu intrusive body rocks

Table 2. major (wt%) and trace element (ppm) data of Qobadlu mafic body

Sample	AGD-01	AGD-0	AGD-0	AGD-	AGD-06	GD-07	RD-01	ARD-02
SiO_2	50.3	52.1	50.3	48.7	46.2	50.9	50.4	50.7
Al_2O_3	18.0	14.4	16.9	17.4	14.6	18.5	16.1	16.4
CaO	9.2	6.8	9.1	9.7	8.9	8.7	8.9	8.8
Fe_2O_3	9.3	10.0	9.9	9.5	9.3	8.7	8.6	8.8
MgO	4.0	3.1	5.8	5.9	6.7	4.7	6.9	5.7
MnO	0.1	0.2	0.2	0.2	0.1	0.1	0.2	0.2
K_2O	0.8	1.5	0.4	0.4	0.7	0.8	1.3	1.4
Na_2O	3.2	2.7	3.1	3.8	2.9	3.4	2.9	2.9
TiO_2	1.8	1.5	1.5	1.8	1.5	1.6	1.1	1.3
LOI	2.9	3.2	2.5	2.5	2.9	2.4	3.6	3.6
Total	99.6	95.5	99.7	99.9	93.8	99.8	100	99.8
Mg#	46.0	38.0	53.8	55.0	58.7	51.3	61.4	56.0
V	273	263	257	206	200	272	195	215
Cr	38	23	187	173	171	104	286	178
Co	27.6	31.1	36.8	30.6	40.9	28.9	37.0	33.6
Ni	32	15	67	52	61	49	83	62
Cu	37	82	44	37	45	46	85	120
Zn	102	130	94	84	100	92	356	241
Rb	26	43	12	18	20	20	34	32
Sr	687	465	525	413	430	548	599	420
Zr	98	139	81	61	87	86	101	151
Nb	4.8	8.3	4.3	8.4	5.2	4.3	4.1	4.7
Cs	0.7	0.6	0.6	0.8	0.5	1.0	0.8	0.6
Ba	291	360	126	120	102	179	383	289
Pb	4.0	10.0	4.0	9.0	15.0	12.0	8.0	7.0
Th	<0.1	1.2	<0.1	<0.1	<0.1	<0.1	<0.1	<0.1
U	0.2	0.9	0.2	0.2	0.1	0.2	0.3	0.5
Y	23.0	29.5	21.1	16.9	14.9	20.3	22.8	26.3
La	16	20	16	15	18	16	16	19
Ce	22	28	18.0	14	11	20	21	29
Pr	2.3	5.2	2.0	3.5	2.2	1.9	2.2	2.8
Nd	11.7	22.6	9.9	16.1	10.0	10.2	10.8	13.4
Sm	2.3	4.8	1.9	2.9	1.7	1.9	2.4	2.7
Eu	1.3	2.1	1.2	1.1	1.0	1.3	1.3	1.3
Gd	3.4	4.6	3.2	2.3	2.4	3.1	3.2	3.5
Tb	0.6	0.8	0.6	0.6	0.4	0.6	0.6	0.7
Dy	3.9	4.1	3.7	3.5	3.5	3.3	3.9	4.3
Er	2.0	2.0	1.6	1.6	1.2	1.5	2.0	2.2
Tm	0.3	0.4	0.3	0.2	0.2	0.3	0.4	0.4
Yb	1.7	2.2	1.7	2.0	1.3	1.6	1.7	2.0
Lu	0.3	0.4	0.3	0.4	0.3	0.2	0.3	0.3
Hf	2.6	3.5	2.3	1.7	1.6	2.4	2.7	3.6
Ta	0.8	1.1	0.7	0.6	0.6	0.7	0.8	0.8
Na_2O+K_2O	4.0	4.3	3.5	4.3	3.6	4.1	4.1	4.3

10.57647/j.ijes.2025.16850

Table 2. major (wt%) and trace element (ppm) data of Qobadlu mafic body (Continued)

Sample	AGD-01	AGD-0	AGD-0	AGD-	AGD-06	GD-07	RD-01	ARD-02
Ce/Pb	5.5	2.8	4.5	1.6	0.7	1.7	2.6	4.1
U/Zr	0.0	0.0	0.0	0.0	0.0	0.0	0.0	0.0
Y/Nb	4.8	3.6	4.9	2.0	2.9	4.7	5.6	5.6
Yb/Ta	2.3	2.0	2.4	3.4	2.3	2.3	2.2	2.5
(La/Nb)n	3	2	4	2	3	4	4	4
(La/Yb)n	6.4	6.1	6.4	5.1	9.3	6.7	6.4	6.4
(La/Sm)n	4.4	2.6	5.4	3.3	6.9	5.4	4.2	4.4
(Ce/Yb)n	3.4	3.3	2.7	1.8	2.2	3.2	3.2	3.8
(Ce/Sm)n	2.3	1.4	2.3	1.2	1.6	2.6	2.1	2.6
(Eu/Yb)n	2.1	2.7	2.0	1.6	2.2	2.4	2.2	1.9
Eu/Eu*	1.38	1.37	1.52	1.32	1.52	1.69	1.43	1.33
(Dy/Yb)	2.3	1.8	2.2	1.7	2.7	2.1	2.3	2.2
(Ba/Nb)	60.6	43.4	29.3	14.3	19.6	41.6	93.4	61.5
(Rb/Ba)	0.1	0.1	0.1	0.2	0.2	0.1	0.1	0.1
(Nb/Ta)	6.4	7.5	6.1	14.5	9.3	6.1	5.2	5.9
∑REE	67.8	97.1	60.3	63.2	53.1	61.8	65.6	81.6

The zircon grains show Th/U ranges from 0.9 to1.9. Nonetheless, these ratios are consistent with those of magmatic zircon. Zircons from AGD-5 sample yield a Concordia age of 99.8 ± 0.65 Ma (MSWD = 0.63, n = 34); and a mean weighted ^{238}U-^{206}Pb age of 98.8 ± 0.65 Ma (MSWD = 0.36, n = 34). Both ages are considered to represent the timing of crystallization of these samples (Fig. 5) Taking error estimates into consideration, the zircon U-Pb ages indicate gabbro was emplaced almost in the Late Cretaceous.

6. Geochemistry

The results of major and trace element analyses for 8 Qobadlu mafic rocks are presented in (Table 2). Mg# = Mg/(Mg+ Fe) varying from 38 to 61.4 and $Na_2O + K_2O$ ranging from 3.54 to 4.31 wt.%. The TiO_2 content changes from 1.08 to 1.78 wt.%. The loss on ignition (LOI) for most samples is <3 wt.%, indicating modest alteration. Rocks samples of the Qobadlu body have low SiO_2 (46.7 – 52.8 wt.%), moderate Fe_2O_3 (9.96 – 8.57 wt.%), CaO (6.79–9.74 wt.%) and high MgO (3.6–9.9 wt.%) with Al_2O_3 (14.30–18.49 wt.%) abundances. The studied samples high contents of MgO and CaO, with only one sample (AGD-2) showing minor amounts of the two latter compounds (4.02 – 6.90 wt. % and 8.7 – 9.7 wt.%). Total alkali versus silica (TAS) classification diagram (Cox et al. 1979) shows that most mafic rocks are gabbro (Fig. 6a). Most mafic rocks have low total alkalis and plot in the calc-alkaline series (Peccerillo and Taylor 1976)(Fig. 6b). In the Harker diagrams (Fig. 7) of major and trace elements exhibited a negative correlation of CaO with SiO_2 and a positive correlation Na_2O with SiO_2. These results show an increase in the content of silica during the secondary process when sodium replaced calcium in the rock. CaO, MgO, MnO and Fe_2O_3 display negative correlation with SiO_2. According to the behavior of the major elements, it can be concluded that the abundant of aluminum oxide in the studied samples imply for being calcic plagioclase as major felsic mineral in these body, which is also consistent with the petrographic evidence. The negative correlation of MgO and MnO with SiO_2 can also indicate olivine and clinopyroxene fractionation from the primary magma and it can also indicate that the Qobadlu mafic rocks were more differentiated of the primary magma. Normalized of the REEs and trace elements of the samples with Primitive mantle shown in (Fig. 8) respectively these rocks are characterized by enrichments in Pb, Sr and K and depletions in Zr, Nb which can indicate the formation of these rocks in the subduction zones and mixing with the constituents of the crust. The samples have variable total REE concentrations, ranging between 53.1 and 81.6 ppm. Comparing basic and basic-intermediate rocks to REE Primitive Mantle (Fig. 8) (Sun and McDonough, 1989), these rocks show enrichments in light rare earth elements (LREEs) relative to heavy rare earth elements and fractionated pattern.The (Eu/Eu^*) positive ratio (1.32-1.69) can be attributed to early crystallization of agioclase and accumulation of plagioclase in these rocks (Lucci et al. 2016).

10.57647/j.ijes.2025.16850

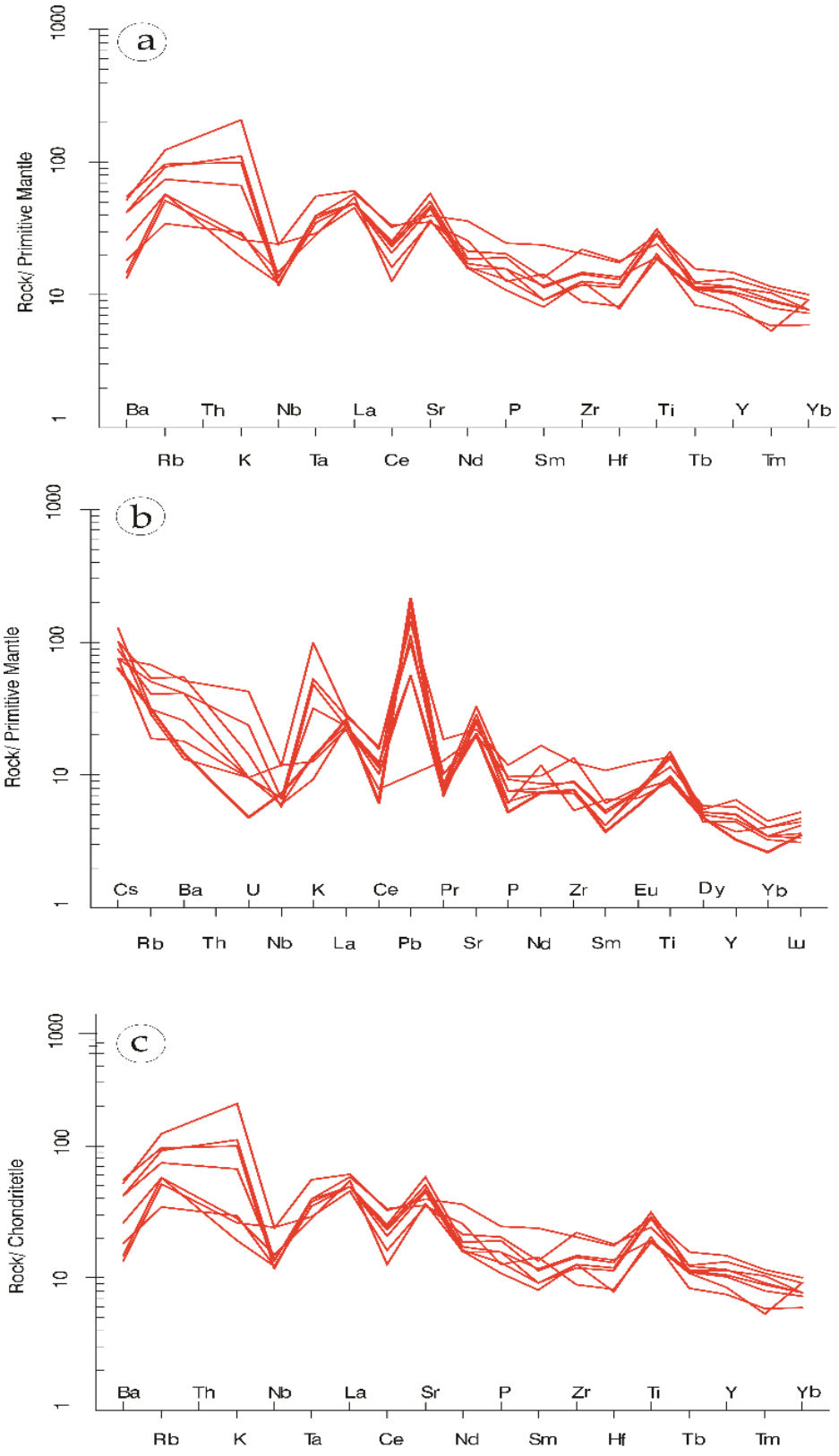


Figure 8. Studied samples normalized to Chondrite and primitive mantle. (Boynton 1984; Sun and McDonough 1989)

10.57647/j.ijes.2025.16850

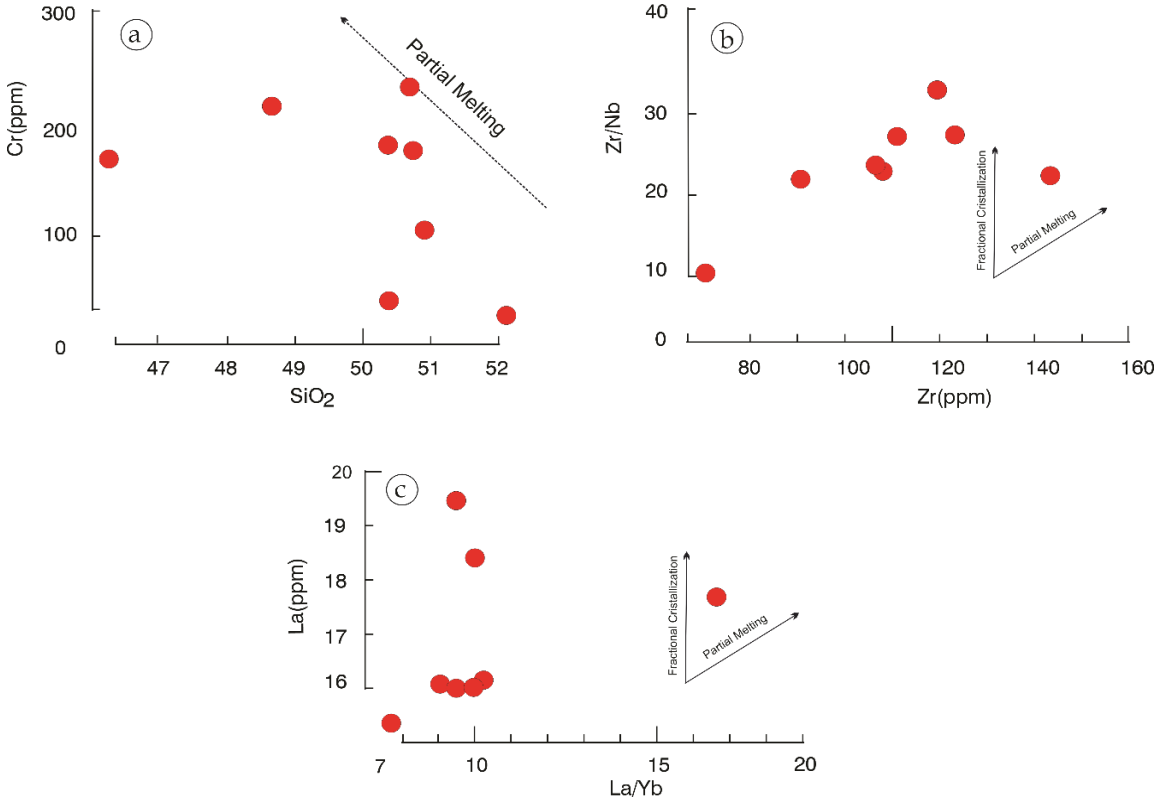


Figure 9. The distributions of mafic rocks in classic discrimination diagrams. (a) Cr versus SiO_2 diagram (Foden et al. 2002), (b,c) Zr/Nb versus Zr and La/Yb versus La (Geng et al. 2009) all samplese show partial melting trend

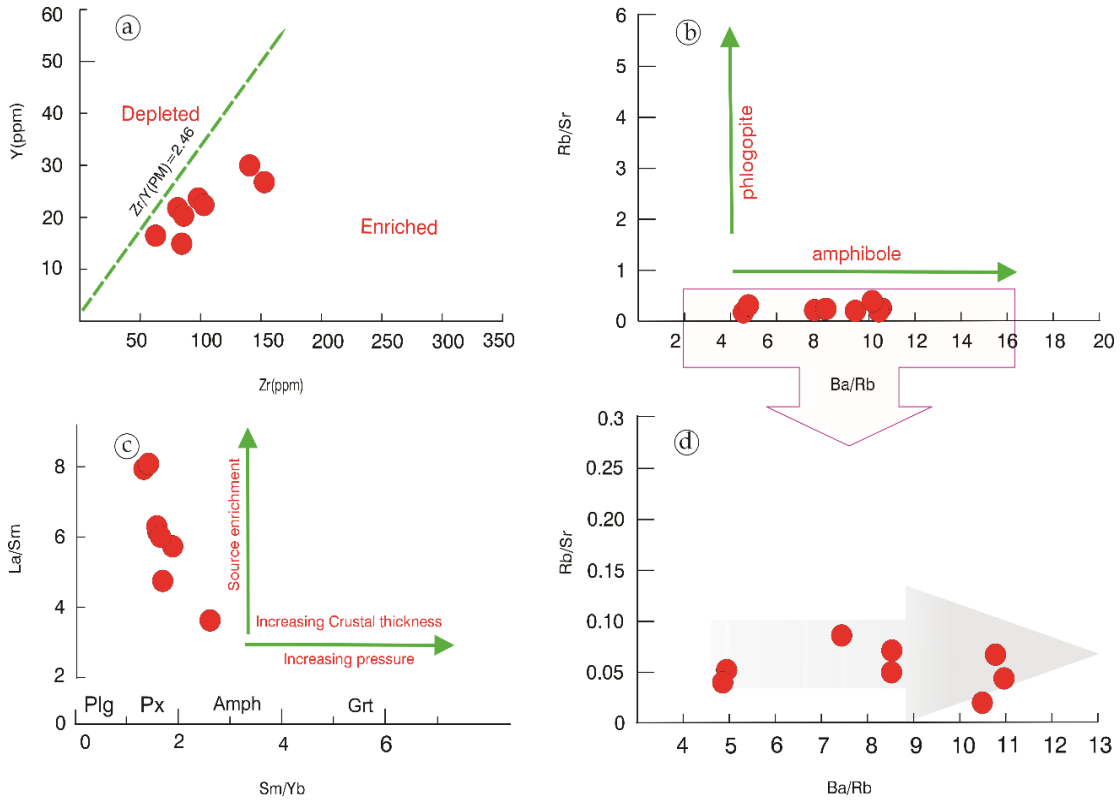


Figure 10. (a) The Zr versus Y diagrams (Abu Hamateh.2005) for the Qobadlu magmatic rocks show the enrichment source for these rocks, (b) The La/Sm versus Sm/Yb diagram (kay et al. 1991, kay and Mpodozis. 2000) for the distributions mantle source, (c) The Ba/Rb versus Rb/Sr diagram show that melting in the mantle is controlled by the amphibole as the remaining phase (Furman and Graham 1999)

10.57647/j.ijes.2025.16850

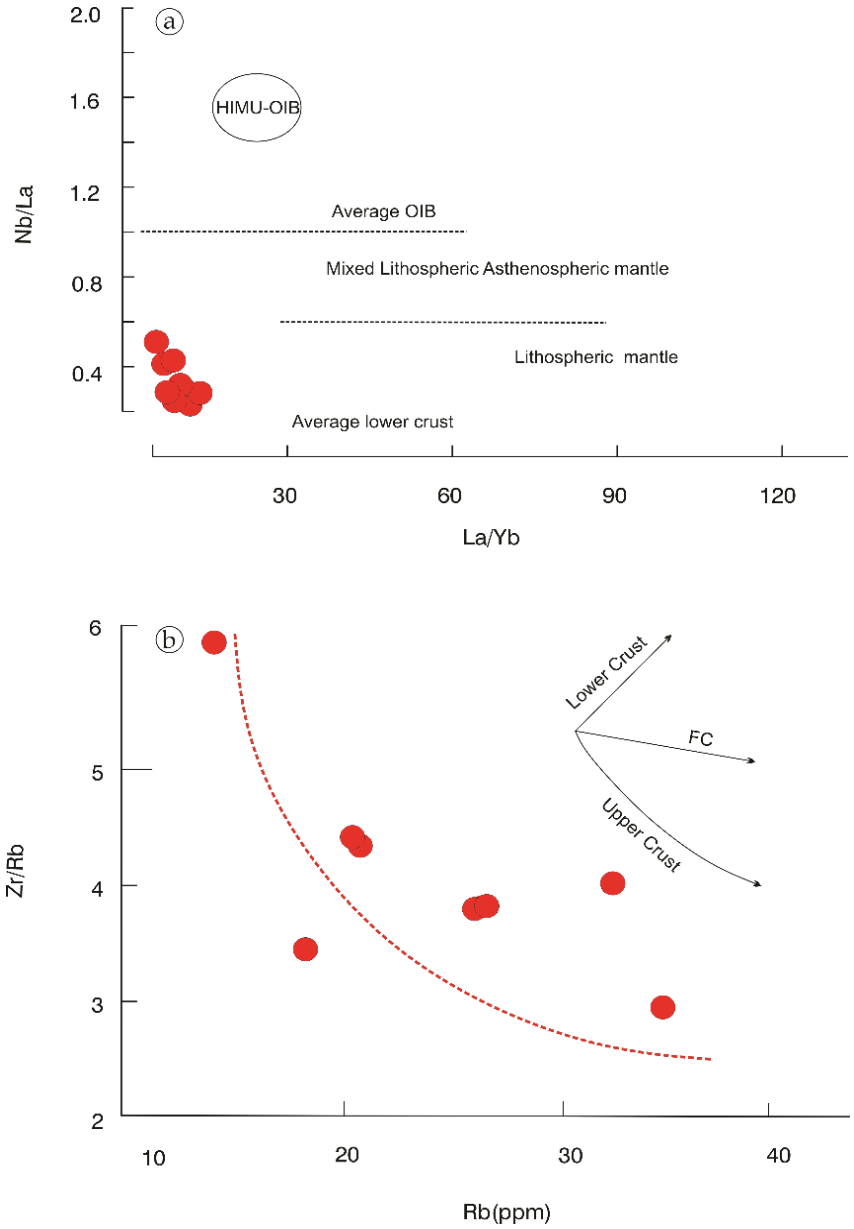


Figure 11. (a) The distributions of mafic rocks Nb/La versus La/Yb, (b) Zr/Rb versus Rb, pattern for Origin Source: OIB (Fitton et al.1997), Lithosphere (Chen et al. 2002), Asthenosphere and Lithosphere (Smithies et al. 2007), OIB-HIMU (Tarney and Weaver 1987)

7. Discussion

In order to distinguish between the processes of partial melting and fractional crystallization role in magma evolution, we can use a couple of different diagrams. Should partial melting be the primary process contributing the magma, one may expect lower concentration of compatible elements in the analyses, which causes a decreasing trend of such elements accompanied with an increasing trend of SiO_2 (Foden et al. 2002; Mišković and Francis 2006). However, Cristallization process tends to lower the concentration of these elements while increasing the abundance of incompatible Fractional elements, LILE and LREE especially K, Rb, Ba, La in the magma bodies (Mišković and Francis 2006) this explains the negative correlation of the sample to SiO_2. The plot of SiO_2 versus Cr (Foden et al. 2002) for the samples from the Qobadlu body indicates the trend of partial melting. This trend is confirmed by the plots of Zr versus Zr/Nb and La/Yb versus La (Geng et al. 2009) this diagrams, showing that the Qobadlu body rocks have been more affected by the partial melting process rather than Fractional Cristallization processes (Fig. 9). However, positive correlation of Mg# and Cr, Ni contents with SiO_2 in studied sample can be suggest in fractional crystallization role in evolution of magma.

10.57647/j.ijes.2025.16850

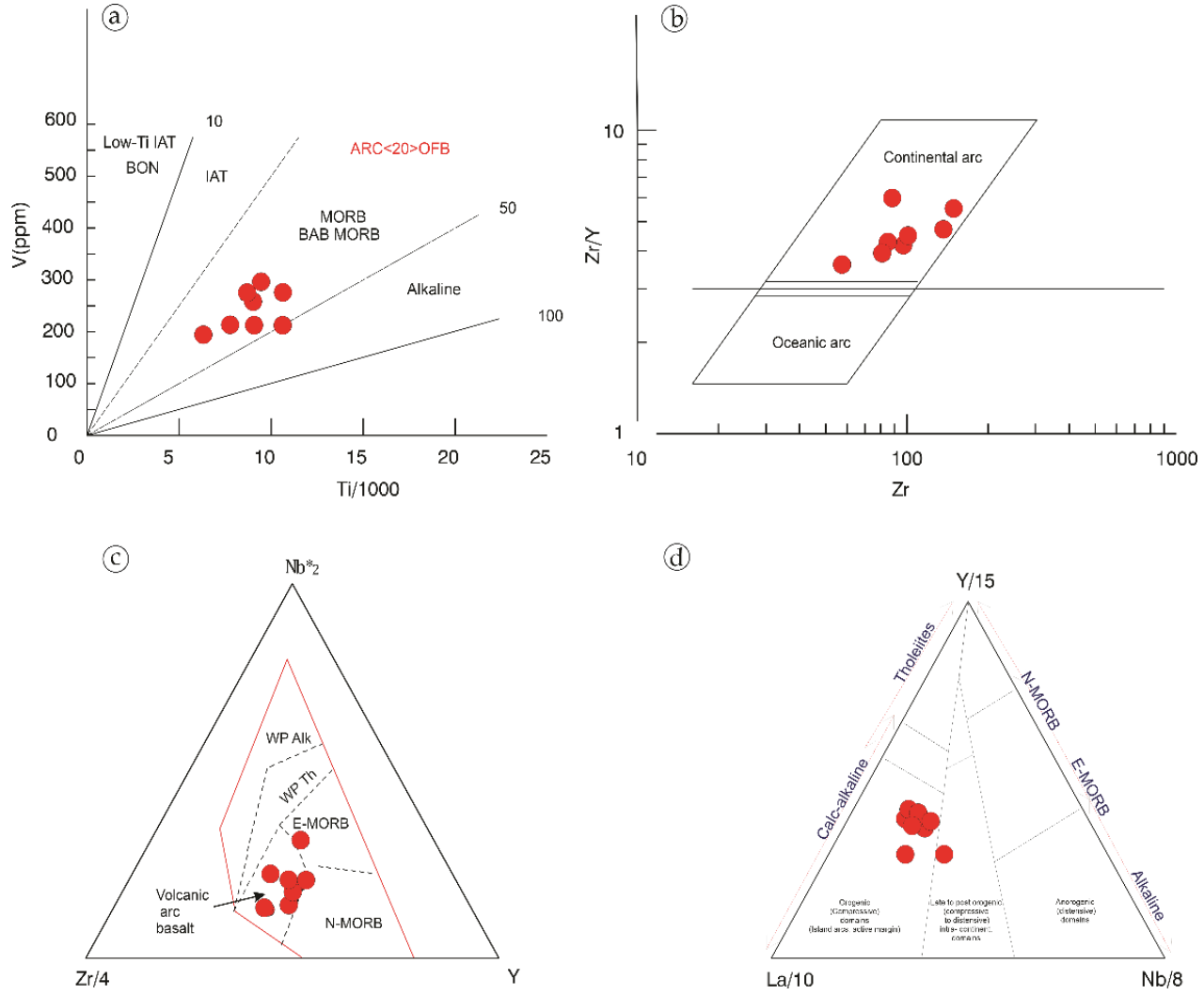


Figure 12. (a) Tectonic discrimination diagram between V and Ti/1000 of (Shervise 1982) Qobadlu samples indicate MORB. (b) The Zr versus Zr/Y diagram (Pearce and Norry 1979) Qobadlu samples indicates Continental volcanic arc magmatism. All samples plot in the field of arc volcanic, Data for MORB and OIB are from (Leroux 1989) and trace element distributions in the rocks from the Qobadlu area, (c)The Nb-Zr -Y plot shows the Volcanic arc. AI-AII = within plate alkaline basalts; B = P-MORB; C = volcanic arc basalt; D = N-MORB after (Meschede 1986) (d) The La/10-Y/15-Nb/8 diagram (Cabanis and Lecolle 1989) Qobadlu Samples indicate active continental margin basalts

Particular minor elements can be used to identify the source of magmas. On the Y versus Zr diagram (Abu-Hamatteh 2005), which is usually used to distinguish between enriched and depleted mantle, the samples from the Qobadlu body fall within the enriched mantle region (Fig. 10a). Source rock composition can be identified from particular index diagrams. An example of such a diagram is the plot of La/Sm versus Sm/Yb (Kay et al. 1991; Kay and Mpodozis 2002). According to this diagram, the pyroxene or even plagioclase constitute the primary constituent minerals of the source rock or the remnants left after partial melting of the source rock. In other words, this characterizes a source of low REEs content in presence of clinopyroxene as the main phase. Absence of garnet in the remnants left upon partial melting of the source rock indicates that the melting occurred at a relatively low pressure. At the same time, the presence of garnet in the source region shows that the pressure in the source zone has ranged from 12 to 15 kbar (Rushmer 1991; Rapp and Watson 1995)(Fig. 10b). In the composition of phlogopite, Ba and Rb have been acknowledged as compatible elements (Adam et al. 1993; Hervig et al. 1995; LaTourrette et al. 1995) while Ba, Rb, and Sr exhibit moderate compatibility with the amphibole. Being in an equilibrium with the phlogopite, the molten matter exhibits a high Rb/Sr ratio coupled with a low Ba/Rb ratio, as compared to the molten matters sourced from amphibole-bearing resources. Moreover, the molten matters sourced from amphibole-bearing resources contain large amounts of Ba and exhibit a high Ba/Rb ratio (Furman and Graham 1999). These criteria can be used to identify the presence/absence of the corresponding phases in the source. Abundance of such incompatible elements as K, Rb, Sr, Ba, Nb may confirm the metasomatic

enrichment in the source zone, thereby helping better understand the melting position. Therefore, these elements can be devised to confirm the presence of phlogopite or amphibole in the source. In some cases, the presence of amphibole and/or phlogopite in the source may indicate the occurrence of fluid- and volatile matter-rich metasomatism prior to melting of these phases. Indeed, an amphibole-rich source reflects the occurrence of carbonate metasomatism while the abundance of the phlogopite indicates the high level of H_2O/CO_2 ratio in the metasomatism agent (Furman and Graham 1999). Based on the Ba/Rb versus Rb/Sr diagram, the process of melting in the mantle is controlled by the amphibole as the remaining phase upon the melting indicate the presence of amphibole mineral in the enriched mantle source. (Fig. 10c). Considering the varying levels of Ba/Rb ratio and fixed value of Nb/La ratio, which characterizes enrichment under the effect of metasomatic fluids. Negative anomalies in elements Nb and to some extent elements with High field strength elements (HFSE) can indicate that these magmas were formed in a subduction zone and during the evolution they were magmatic mixed with the constituents of the crust, as well as the higher values of the elements on the left side of the spider diagram. According to (Pearce et al. 1997), the rocks formed upon consolidation of the magma derived from the subduction zone exhibit Nb contents below 15 ppm. For all samples taken from the Qobadlu body, this parameter fell below 10 ppm. The magmas associated with the lithospheric mantle exhibit La/Nb ratios above 1, while the same ratio is about 0.7 for the magmas derived from asthenospheric mantle (DePaolo and Daley 2000). When it comes to the rocks associated with active continental margin, this ratio exceeds 2.2, while it measured at less-than-one values in intracontinental magmas. Contamination of magma with the lithospheric mantle as it escalates tends to lower this ratio. For this area, the magma mixing phenomenon was characterized by a ratio in the range of 0.7 to 1 (Van Kranendonk et al. 2007). In the rocks of the Qobadlu body, except for a single sample (AGD-5), the ratio was found to exceed 2.2, being well in agreement with the fact that the body is developed on an active continental margin. In most of the analyzed samples, the ratio exceeded 30. According to (Appel 1998) Ba/Nb ratio above 30 can characterize the melts sourced from metasomatized mantle wedge on top of a subducting slab – a fact that is well in agreement with the features of an active continental margin (Fitton et al. 1997). In all samples from the Qobadlu body, the $(La/Yb)_N$ and $(Dy/Yb)_N$ ratios were slightly high (11.5 – 1.5 and 1.7 – 1.1, respectively), confirming the enrichment by LREEs. Enrichment by U, Cs, and Pb can be attributed to the contamination of magma with the crust components. Trying to identify the source mantle of magmas based on the La/Yb versus Nb/La diagrams, the samples were plotted in the vicinity of the lower crust, showing that the parent magma might have been contaminated with the upper crust (Fig. 11). In the Rb versus Zr/Rb diagram for the plutonic samples of the Qobadlu body, contamination of magma with the upper crust was confirmed. All of these anomalies show that the studied samples have been formed following partial melting of a spinel lherzolitic source. Subsequently, upon the release of subduction fluids through the subducting edge and migration of these fluids into the mantle wedge, the partial melting in this part of the mantle has led to the formation gabbro magmas that constitute the Qobadlu body.

7.1. Geodynamics and Tectonic setting

On the Ti/1000 versus V diagram (Shervais 1982) the samples fall in the region corresponding to back-arc basalt (BAB). On the Zr versus Zr/Y diagram (Fitton et al. 1997) however, the Qobadlu gabbro body falls in the region corresponding to continental arc-associated environment (Pearce and Norry 1979). On the La/10-Y/15-Nb/8 diagram presented by (Cabanis and Lecolle 1989), all samples fall in the range of magmas with a calc-alkaline source corresponding to active continental margin environments (Fig. 12).

Figure 12. (a) Tectonic discrimination diagram between V and Ti/1000 of (Shervise 1982) Qobadlu samples indicate MORB. (b) The Zr versus Zr/Y diagram (Pearce and Norry 1979) Qobadlu samples indicates Continental volcanic arc magmatism. All samples plot in the field of arc volcanic, Data for MORB and OIB are from (Leroux 1989) and trace element distributions in the rocks from the Qobadlu area, (c)The Nb-Zr -Y plot shows the Volcanic arc. AI-AII = within plate alkaline basalts; B = P-MORB; C = volcanic arc basalt; D = N-MORB after (Meschede 1986) (d) The La/10-Y/15-Nb/8 diagram (Cabanis and Lecolle 1989) Qobadlu Samples indicate active continental margin basalts. The SaSZ hosts metamorphic rocks (metabasite and metasedimentary), volcanic rocks, and granite bodies with Mesozoic ages. Based on the geochemistry of the magmatic rocks, this zone has been divided into three main parts (i.e., central, northern, and southern parts(Azizi and Stern 2019)The main Jurassic magmatism (Tavakoli et al. 2020; Tavakoli et al. 2021)has been concentrated in the central part of SaSZ, while the rocks in the northern part are younger than those in the central and southern parts, and the granitoids get younger as one move toward north. Cretaceous successions in the northern part of the SaSZ include volcanic rocks of basalt-andesite, sub-volcanic tuffs, agglomerate and breccia, and interbedding rocks in the form of black shale and sandstone, which overly the Cadomian crust and are

heterogeneously covered by Cretaceous limestones (Eftekharnejad 1981; Kazmin et al. 1986; Alavi 1994; Hosseiny 1999; Baharifar et al. 2004) The sediments in this part Metamorphed in green schist to amphibolie facies. (Mohajjel et al. 2003; Baharifar et al. 2004; KHAN and Ziaei 2007; Davoudian et al. 2008) and its Jurassic volcanic rocks exhibit calc-alkaline to tholeiitic characters (Eftekharnejad 1981; Kazmin et al. 1986; Alavi 1994; Ghasemi and Talbot 2006) which shows that they have source from an active continental margin during a subduction event. New investigations confirm that the Neotethys subduction below the SaSZ has started in Early Cretaceous followed by the Arabian – Iranian plate collision in Eocene (37 – 40 Ma). The coexisting granites with the tectonics along the Zagros suture zone in Baneh have been dated back to 37 – 40 Ma, indicating the occurrence of the collision in northwest of Iran in the Late Eocene. Due to the large gap of magmatism between Carboniferous (330 Ma) and Early Cretaceous (110 Ma) in the northern part of SaSZ (Gholipour et al. 2021) there is no evidence of the subduction of the oceanic lithosphere in the SaSZ until Early Cretaceous (Fig. 13). Although some evidence of Cretaceous subduction in SaSZ have been reported previously (Azizi and Jahangiri 2008, Gholipour et al. 2021) Early Cretaceous andesites and I-type granites in the northern part of SaSZ in Saqqez which are formed on an active continental margin, indicate the subduction of Neotethys under the northern SaSZ was in Early Cretaceous (Gholipour et al. 2021). During this subduction created horst-and-graben structures development across the continental crust. injection of hot magma with a calc-alkaline to slightly tholeiitic composition resulted in the thinning of the crust. During Cretaceous, in these fault-dominated extended basins, sub-marine volcanic activities occurred. Extensional back-arc basin of Khoy basin, and the fault-dominated extensional basin in Azerbaijan have been attributed to this subduction (Moayyed and Moazzen 2002). The thinning and formation of fractures provide suitable accommodation for the intrusion of hot magma, which leads to the intrusion of metasomatized magma and formation of the Qobadlu mafic body.

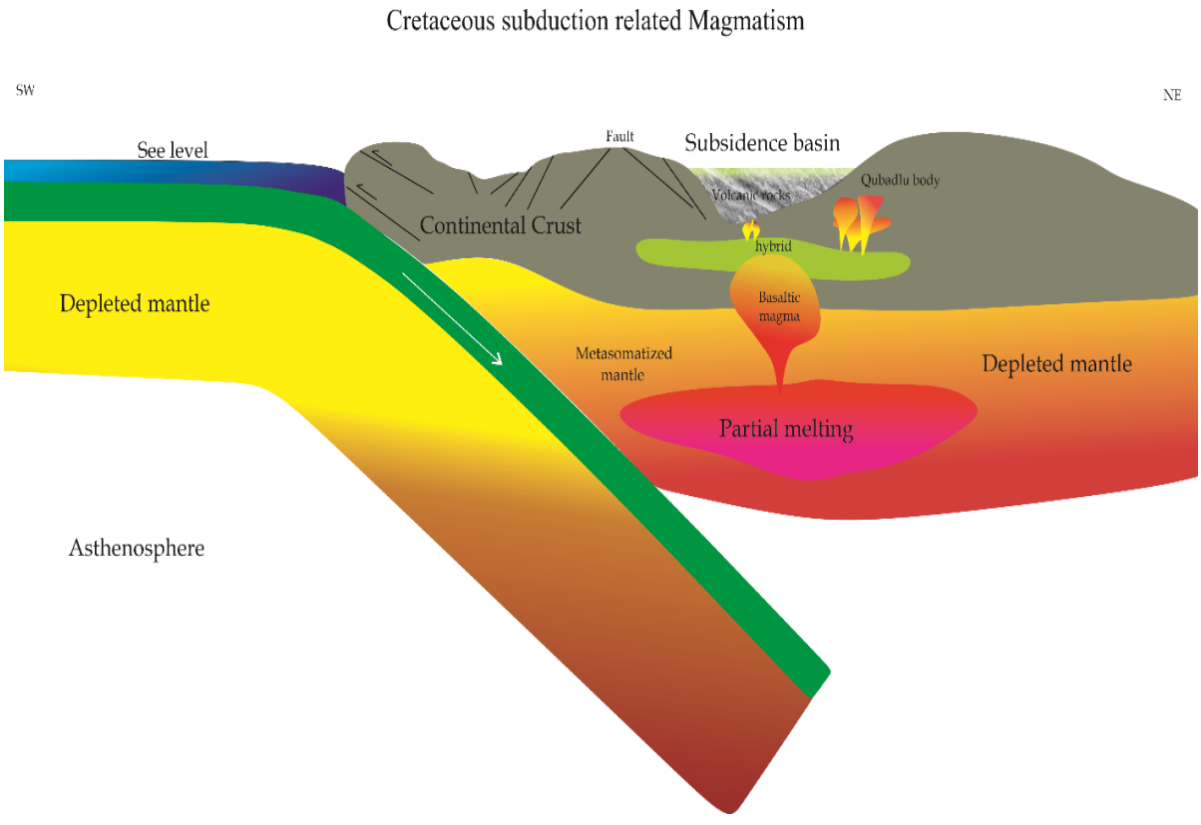


Figure 13. Schematic representation of Cretaceous subduction related Magmatism in the Northern Sanandaj Sirjan Zone

8. Conclusion

In the north of the Sanandaj-Sirjan zone, magmatic activities have occurred in three main periods: in the first period, Neoproterozoic-Paleozoic granites and igneous rocks have been formed. The second stage occurred around 331 Ma, and the Carboniferous granites between the Tabriz and Zagros faults belong to this period. The third group includes felsic and basic Cretaceous intrusive

and volcanic rocks that Qobadlu body is in this group. Based on Zircon dating of the Qobadlu mafic body with the combination of olivine gabbro to gabbro and gabbro-diorite during the Upper Cretaceous period penetrated into the dark colored shales, sandstones and volcanic rocks of the Lower Cretaceous and caused silicification of the shales. The enrichment of LILE and LREE elements indicates an enriched mantle origin for the parent magma. The diagrams such as Ba/Rb, Zr/Rb indicate the enrichment of the origin of these rocks and the formation of amphibole minerals in the origin of lherzolite mantle. Considering the evidence of Lithostratigraphy, the proposed tectonic model for the Qobadlu body can be summarized as follows. According to the model proposed in this research for the Qobadlu body, the subduction of the Neotethys under the northwest block of Iran has caused the formation of rocks in the region, as a result of this subduction, the forearc basin horst and graben is developed near the trench zone without magmatic activity. In contrast, flare-ups of a calc-alkaline magmatic activity with a slight tendency toward tholeiitic with basaltic and andesitic composition occurred around the Trench. The result is the production of felsic magma in the upper crust. Thinning of the crust away from the subduction zone to create a back-arc basin-like regime causes hot asthenospheric melts to rise, leading to the production of tholeiitic to peralkaline magmas, for example reported in the western Pacific.

Authors Contribution
All the authors have participated sufficiently in the intellectual content, conception, and design of this work or the analysis and interpretation of the data (when applicable), as well as the writing of the manuscript.

Availability of data and materials
The data that support the findings of this study are available from the corresponding author upon reasonable request.

Conflict of interest
The author states that there is no conflict of interest.

References

Abdolahadi, A., Sheikhzakariaee, S. J., Yazdi, A. and Mousavi, S. Z. 2025. Plio-Quaternary Adakite Genesis and Post-collisional Processes: Whole Rock Constraints and Sr, Nd Isotopic Compositions in Alborz Magmatic Belt, Ardabil, Iran, *Journal of Mining and Environment*, 16(2):737–765. DOI: https://doi.org/10.22044/jme.2024.14781.2801

Abu-Hamatteh, Z. 2005. Geochemistry and petrogenesis of mafic magmatic rocks of the Jharol Belt, India: geodynamic implication, *Journal of Asian Earth Sciences*, 25:557–581. DOI: https://doi.org/10.1016/j.jseaes.2004.05.006

Adam, J., Green, T. and Sie, S. 1993. Proton microprobe determined partitioning of Rb, Sr, Ba, Y, Zr, Nb and Ta between experimentally produced amphiboles and silicate melts with variable F content, *Chemical Geology*, 109:29–49. DOI: https://doi.org/10.1016/0009-2541(93)90060-V

Ahmadi Khalaji, A. and Tahmasbi, Z. 2015. Mineral chemistry of garnet in pegmatite and metamorphic rocks in the Hamedan area, *Journal of Economic Geology*, 7:243–258. DOI: https://doi.org/10.22067/econg.v7i2.31041

Alavi-Naini, M. and Shahrabi, M. 1975. Geological map of Maragheh. 1:100,000 series, Sheet 5265, Ministry of Industry and Mines, *Geological Survey of Iran*, Tehran.

Alavi, M. 1994. Tectonics of the Zagros orogenic belt of Iran: new data and interpretations, *Tectonophysics*, 229:211–238.

Ali Rajabzadeh, M. and Esmaeili, S. 2014. Investigation on protolith and tectonic setting of metamorphic rocks in the Surian complex using petrographic and geochemical data, *Petrology (2228-5210)*, 5.

Appel, V. 1998. Geological, geochronological and Pb isotopic constraints on the age and origin of the Mount Nansen epithermal Au-Ag vein deposit, eastern Dawson Range, Yukon, *Unpublished B Sc Thesis, University of British Columbia, Vancouver, BC*.

Arvin, M., Pan, Y., Dargahi, S., Malekizadeh, A. and Babaei, A. 2007. Petrochemistry of the Siah-Kuh granitoid stock southwest of Kerman, Iran: Implications for initiation of Neotethys subduction, *Journal of Asian Earth Sciences*, 30:474–489. DOI: https://doi.org/10.1016/j.jseaes.2007.01.001

Ashrafi, N., Dabiri, R. and Jahangiri, A. 2024. Some chemical variations in biotite, phlogopite, and muscovite, considering their tectonic setting, *Geopersia*, 14(2):307–332. DOI: https://doi.org/10.22059/geope.2024.373882.648749

Azizi, H. and Asahara, Y. 2013. Juvenile granite in the Sanandaj–Sirjan Zone, NW Iran: late Jurassic–early Cretaceous arc–continent collision, *International Geology Review*, 55:1523–1540. DOI: https://doi.org/10.1080/00206814.2013.782959

Azizi, H., Asahara, Y., Mehrabi, B. and Chung, S. L. 2011. Geochronological and geochemical constraints on the petrogenesis of high-K granite from the Suffi abad area, Sanandaj-Sirjan Zone, NW Iran, *Geochemistry*, 71:363–376. DOI: https://doi.org/10.1016/j.chemer.2011.06.005

Azizi, H. and Jahangiri, A. 2008. Cretaceous subduction-related volcanism in the northern Sanandaj-Sirjan Zone, Iran, *Journal of Geodynamics*, 45:178–190. DOI: https://doi.org/10.1016/j.jog.2007.11.001

Azizi, H., Kazemi, T. and Asahara, Y. 2017. A-type granitoid in Hasansalaran complex, northwestern Iran: Evidence for extensional tectonic regime in northern Gondwana in the Late Paleozoic, *Journal of Geodynamics*, 108:56–72. DOI: https://doi.org/10.1016/j.jog.2017.05.003

Azizi, H., Najari, M., Asahara, Y., Catlos, E. J., Shimizu, M. and Yamamoto, K. 2015. U–Pb zircon ages and geochemistry of Kangareh and Taghiabad mafic bodies in northern Sanandaj–Sirjan Zone, Iran: evidence for intra-oceanic arc and back-arc tectonic regime in Late Jurassic, *Tectonophysics*, 660:47–64. DOI: https://doi.org/10.1016/j.tecto.2015.08.008

Azizi, H., Nouri, F., Stern, R. J., Azizi, M., Lucci, F., Asahara, Y., Zarinkoub, M. H. and Chung, S. L. 2020. New evidence for Jurassic continental rifting in the northern Sanandaj Sirjan Zone, western Iran: the Ghalaylan seamount, southwest Ghorveh, *International Geology Review*, 62:1635–1657. DOI: https://doi.org/10.1080/00206814.2018.1535913

Azizi, H. and Stern, R. J. 2019. Jurassic igneous rocks of the central Sanandaj–Sirjan zone (Iran) mark a propagating continental rift, not a magmatic arc, *Terra Nova*, 31:415–423. DOI: https://doi.org/10.1111/ter.12404

Baharifar, A., Moinevaziri, H., Bellon, H. and Piqué, A. 2004. The crystalline complexes of Hamadan (Sanandaj–Sirjan zone, western Iran): metasedimentary Mesozoic sequences affected by Late Cretaceous tectono-metamorphic and plutonic events, *Comptes Rendus Geoscience*, 336:1443–1452.
DOI: https://doi.org/10.1016/j.crte.2004.09.014

Bayati, M., Esmaeily, D., Maghdour-Mashhour, R., Li, X.-H. and Stern, R. J. 2017. Geochemistry and petrogenesis of Kolah-Ghazi granitoids of Iran: Insights into the Jurassic Sanandaj-Sirjan magmatic arc, *Geochemistry*, 77:281–302.
DOI: http://dx.doi.org/10.1016/j.chemer.2017.02.003

Berberian, F. and Berberian, M. 1981. Tectono-plutonic episodes in Iran, *Zagros Hindu Kush Himalaya Geodynamic Evolution*, 3:5–32.

Boynton, W. V. 1984. Cosmochemistry of the rare earth elements: meteorite studies. In: *Developments in Geochemistry*, vol. 2. Elsevier, pp. 63–114.
DOI: https://doi.org/10.1016/B978-0-444-42148-7.50008-3

Cabanis, B. and Lecolle, M. 1989. The La/10–Y/15–Nb/8 diagram: A tool for distinguishing volcanic series and discovering crustal mixing and/or contamination, *Comptes Rendus de l'Academie des Sciences, Serie 2, Science de la Terre*, 309:20.

Chen, B., Jahn, B.-M. and Wei, C. 2002. Petrogenesis of Mesozoic granitoids in the Dabie UHP complex, Central China: trace element and Nd–Sr isotope evidence, *Lithos*, 60:67–88.
DOI: https://doi.org/10.1016/S0024-4937(01)00077-9

Cox, K., Bell, J. and Pankhurst, R. 1979. Fractionation in igneous processes. In: The Interpretation of Igneous Rocks, *Springer*, pp. 1–11.

Dabiri, R., Akbari-Mogaddam, M. and Ghaffari, M. 2018. Geochemical evolution and petrogenesis of the Eocene Kashmar granitoid rocks, NE Iran: Implications for fractional crystallization and crustal contamination processes, *Iranian Journal of Earth Sciences*, 10(1):68–77.

Davoudian, A., Genser, J., Dachs, E. and Shabanian, N. 2008. Petrology of eclogites from north of Shahrekord,

Davoudian, A., Genser, J., Dachs, E. and Shabanian, N. 2008. Petrology of eclogites from north of Shahrekord, Sanandaj-Sirjan zone, Iran, *Mineralogy and Petrology*, 92:393–413.
DOI: https://doi.org/10.1007/s00710-007-0204-6

Davoudian, A. R., Genser, J., Neubauer, F. and Shabanian, N. 2016. ^40Ar/^39Ar mineral ages of eclogites from North Shahrekord in the Sanandaj–Sirjan Zone, Iran: implications for the tectonic evolution of Zagros orogen, *Gondwana Research*, 37:216–240.
DOI: https://doi.org/10.1016/j.gr.2016.05.013

DePaolo, D. J. and Daley, E. E. 2000. Neodymium isotopes in basalts of the southwest basin and range and lithospheric thinning during continental extension, *Chemical Geology*, 169:157–185.
DOI: https://doi.org/10.1016/S0009-2541(00)00261-8

Eftekharnejad, J. 1981. Tectonic division of Iran with respect to sedimentary basins, *Journal of the Iranian Petroleum Society*, 82:19–28.

Fazlnia, A. 2016. Geochemistry and tectonomagmatic setting of the Kharaju gabbroic intrusions (South Azarshahr, East Azerbaijan province), *Petrological Journal*, 7:127–144.
DOI: https://doi.org/10.22108/ijp.2016.21240

Fazlnia, A., Schenk, V., van der Straaten, F. and Mirmohammadi, M. 2009. Petrology, geochemistry, and geochronology of trondhjemites from the Qori Complex, Neyriz, Iran, *Lithos*, 112:413–433.
DOI: https://doi.org/10.1016/j.lithos.2009.03.047

Fitton, J., Saunders, A., Norry, M., Hardarson, B. and Taylor, R. 1997. Thermal and chemical structure of the Iceland plume, *Earth and Planetary Science Letters*, 153:197–208.
DOI: https://doi.org/10.1016/S0012-821X(97)00170-2

Foden, J., Song, S. H., Turner, S., Elburg, M., Smith, P., Van der Steldt, B. and Van Penglis, D. 2002. Geochemical evolution of lithospheric mantle beneath SE South Australia, *Chemical Geology*, 182:663–695.
DOI: https://doi.org/10.1016/S0009-2541(01)00347-3

Furman, T. and Graham, D. 1999. Erosion of lithospheric mantle beneath the East African Rift system: geochemical evidence from the Kivu volcanic province. In: *Developments in Geotectonics*, vol. 24. Elsevier, pp. 237–262.
DOI: https://doi.org/10.1016/S0419-0254(99)80014-7

Geng, H., Sun, M., Yuan, C., Xiao, W., Xian, W., Zhao, G., Zhang, L., Wong, K. and Wu, F. 2009. Geochemical, Sr–Nd and zircon U–Pb–Hf isotopic studies of Late Carboniferous magmatism in the West Junggar, Xinjiang: Implications for ridge subduction, *Chemical Geology*, 266:364–380.
DOI: https://doi.org/10.1016/j.chemgeo.2009.07.001

Ghadirzadeh, A. and Anvari, A. 1998. Azarshahr geological map, scale 1:100,000, *Geological Survey of Iran (GSI)*.

Ghasemi, A. and Talbot, C. J. 2006. A new tectonic scenario for the Sanandaj–Sirjan Zone (Iran), *Journal of Asian Earth Sciences*, 26:683–693.
DOI: https://doi.org/10.1016/j.jseaes.2005.01.003

Gholipour, S., Azizi, H., Masoudi, F., Asahara, Y. and Tsuboi, M. 2021. Zircon U–Pb ages, geochemistry, and Sr–Nd isotope ratios for early Cretaceous magmatic rocks, southern Saqqez, northwestern Iran, *Geochemistry*, 81:125687.
DOI: https://doi.org/10.1016/j.chemer.2020.125687

Gill, J.B., 1976. Composition and age of Lau Basin and Ridge volcanic rocks: Implications for evolution of an interarc basin and remnant arc, *Geological Society of America Bulletin*, 87:1384–1395.
DOI: https://doi.org/10.1130/0016
7606(1976)87%3C1384:CAAOLB%3E2.0.CO;2

Hassanzadeh, J., Stockli, D. F., Horton, B. K., Axen, G. J., Stockli, L. D., Grove, M., Schmitt, A. K. and Walker, J. D. 2008. U–Pb zircon geochronology of late Neoproterozoic–Early Cambrian granitoids in Iran: Implications for paleogeography, magmatism, and exhumation history of Iranian basement, *Tectonophysics*, 451:71–96.
DOI: https://doi.org/10.1016/j.tecto.2007.11.062

Hassanzadeh, J. and Wernicke, B. 2022. Comment on "Neotethyan subduction ignited the Iran arc and back-arc differently" by Shafaii Moghadam et al. (2020), *Authorea Preprints*.
DOI: https://doi.org/10.1002/essoar.10503665.1

Hassanzadeh, J. and Wernicke, B. P. 2016. The Neotethyan Sanandaj–Sirjan zone of Iran as an archetype for passive margin–arc transitions, *Tectonics*, 35:586–621.
DOI: https://doi.org/10.1002/2015TC003926

Hervig, R. L., Williams, L. B., Kirkland, I. K. and Longstaffe, F. J. 1995. Oxygen isotope microanalyses of diagenetic quartz: possible low-temperature occlusion of pores, *Geochimica et Cosmochimica Acta*, 59:2537–2543.
DOI: https://doi.org/10.1016/0016-7037(95)00148-4

Hosseiny, M. 1999. Geological map of Sanandaj, scale 1:100,000, Geological Survey of Iran.

Hunziker, D., Burg, J.-P., Bouilhol, P. and von Quadt, A. 2015. Jurassic rifting at the Eurasian Tethys margin: Geochemical and geochronological constraints from granitoids of North Makran, southeastern Iran, *Tectonics*, 34:571–593.
DOI: https://doi.org/10.1002/2014TC003768

Jahangiri, A. 2007. Post-collisional Miocene adakitic volcanism in NW Iran: geochemical and geodynamic implications, *Journal of Asian Earth Sciences*, 30:433–447.
DOI: https://doi.org/10.1016/j.jseaes.2006.11.008

Kay, S. M. and Mpodozis, C. 2002. Magmatism as a probe to the Neogene shallowing of the Nazca plate beneath the modern Chilean flat-slab, *Journal of South American Earth Sciences*, 15:39–57.
DOI: https://doi.org/10.1016/S0895-9811(02)00005-6

Kay, S. M., Mpodozis, C., Ramos, V. and Munizaga, F. 1991. Magma source variations for mid- to late Tertiary volcanic rocks erupted over a shallowing subduction zone and through a thickening crust in the Main Andean Cordillera (28–33°S), *Andean Magmatism and its Tectonic Setting, Geological Society of America Special Paper*, 265:113–137.
DOI: https://doi.org/10.1130/SPE265-p113

Kazemi Koohbanani, S., Sheikhzakariee, S. J., Emami, M. H. and Dabiri, R. 2018. Geochemistry and tectonic setting of Kohe Siah volcanoes, North Qorveh, Sanandaj, Iran, *Open Journal of Geology*, 8(5):474–488.
DOI: https://doi.org/10.4236/ojg.2018.85028

Kazmin, V., Ricou, L.-E. and Sbortshikov, I. 1986. Structure and evolution of the passive margin of the eastern Tethys, *Tectonophysics*, 123:153–179.
DOI: https://doi.org/10.1016/0040-1951(86)90196-4

Kent, A.J., Peate, D.W., Newman, S., Stolper, E.M. and Pearce, J.A., 2002. Chlorine in submarine glasses from the Lau Basin: Seawater contamination and constraints on the composition of slab-derived fluids, *Earth and Planetary Science Letters*, 202:361–377.
DOI: https://doi.org/10.1016/S0012-821X(02)00786-0

Khan, N. E. A. and Ziaei, H. R. 2007. Using multivariable statistical methods to separation and detection of lithologic units in ETM+ satellite images, case study: Outcrops in the south of Ab-Poneh village, Tiran (west Isfahan).

Kouchi, Y., Obara, H., Fujimoto, T., Orihashi, Y., Haruta, Y. and Yamamoto, K. 2015. Zircon U–Pb dating by 213 nm Nd:YAG laser ablation inductively coupled plasma mass spectrometry: Optimization of the analytical condition to use NIST SRM 610 for Pb/U fractionation correction, *Chikyu Kagaku*, 49:19–35.
DOI: https://doi.org/10.14934/chikyukagaku.49.19

LaTourrette, T., Hervig, R. L. and Holloway, J. R. 1995. Trace element partitioning between amphibole, phlogopite, and basanite melt, *Earth and Planetary Science Letters*, 135:13–30.
DOI: https://doi.org/10.1016/0012-821X(95)00146-4

Lechmann, A., Burg, J.-P., Ulmer, P., Mohammadi, A., Guillong, M. and Faridi, M. 2018. From Jurassic rifting to Cretaceous subduction in NW Iranian Azerbaijan: geochronological and geochemical signals from granitoids, *Contributions to Mineralogy and Petrology*, 173:1–16.
DOI: https://doi.org/10.1007/s00410-018-1532-8

Leroux, M. V. 1989. Mineralogical and geochemical investigation of the cordierite–anthophyllite rocks at Star Lake, near Sherridon, Manitoba.

Lucci, F., Miri, M., Saki, A., White, J. C., Della Ventura, G. and Azizi, H. 2023. The Middle Jurassic Cheshmeh-Ghasaban High-Mg gabbro (Hamedan, NW Iran): A plume-influenced intracontinental rifting event?, *Geochemistry*, 83:126011.
DOI: https://doi.org/10.1016/j.chemer.2023.126011

Lucci, F., Rossetti, F., White, J. C., Moghadam, H. S., Shirzadi, A. and Nasrabady, M. 2016. Tschermak fractionation in calc-alkaline magmas: the Eocene Sabzevar volcanism (NE Iran), *Arabian Journal of Geosciences*, 9:1–12.
DOI: https://doi.org/10.1007/s12517-016-2598-0

Ludwig, K., 2012. Isoplot: A Geochronological Toolkit for Microsoft Excel, Berkeley Geochronology Center, *Special Publication*, 5:75.

Maghdour-Mashhour, R., Hayes, B., Pang, K.-N., Bolhar, R., Shabani, A. A. T. and Elahi-Janatmakan, F. 2021. Episodic subduction initiation triggered Jurassic magmatism in the Sanandaj–Sirjan zone, Iran, *Lithos*, 396:106189.
DOI: https://doi.org/10.1016/j.lithos.2021.106189

Malek-Mahmoudi, F., Davoudian, A. R., Shabanian, N., Azizi, H., Asahara, Y., Neubauer, F. and Dong, Y. 2017. Geochemistry of metabasites from the North Shahrekord metamorphic complex, Sanandaj-Sirjan Zone: Geodynamic implications for the Pan-African basement in Iran, *Precambrian Research*, 293:56–72.
DOI: https://doi.org/10.1016/j.precamres.2017.03.003

Meschede, M. 1986. A method of discriminating between different types of mid-ocean ridge basalts and continental tholeiites with the Nb–Zr–Y diagram, *Chemical Geology*, 56:207–218.
DOI: https://doi.org/10.1016/0009-2541(86)90004-5

Mišković, A. and Francis, D. 2006. Interaction between mantle-derived and crustal calc-alkaline magmas in the petrogenesis of the Paleocene Sifton Range volcanic complex, Yukon, Canada, *Lithos*, 87:104–134.
DOI: https://doi.org/10.1016/j.lithos.2005.05.007

Moayyed, M. and Moazzen, M. 2002. A new view to the Paleo-Tethys suture line position in Iran, *Geological Society*, 9:716–717.

Mohajjel, M., Fergusson, C. and Sahandi, M. 2003. Cretaceous–Tertiary convergence and continental collision, Sanandaj–Sirjan zone, western Iran, *Journal of Asian Earth Sciences*, 21:397–412.
DOI: https://doi.org/10.1016/S1367-9120(02)00035-4

Mohajjel, M. and Fergusson, C. L. 2000. Dextral transpression in Late Cretaceous continental collision, Sanandaj–Sirjan zone, western Iran, *Journal of Structural Geology*, 22:1125–1139.
DOI: https://doi.org/10.1016/S0191-8141(00)00023-7

Mollai, H., Dabiri, R., Torshizian, H. A., Pe-Piper, G. and Wang, W. E. 2021. Upper Neoproterozoic garnet-bearing granites in the Zeber-Kuh region from east central Iran microplate: Implications for the magmatic evolution in the northern margin of Gondwanaland, *Geologica Carpathica*, 72(6):461–481.
DOI: http://dx.doi.org/10.31577/GeolCarp.72.6.2

Mousivand, F., Rastad, E., Meffre, S., Peter, J. M., Solomon, M. and Zaw, K. 2011. U–Pb geochronology and Pb isotope characteristics of the Chahgaz volcanogenic massive sulphide deposit, southern Iran, *International Geology Review*, 53:1239–1262.
DOI: https://doi.org/10.1080/00206811003783364

Nasr-Esfahani, A.-K. 2012. Tectonic setting of metabasites of the Neo-Tethyan oceanic remains in Sanandaj–Sirjan structural zone, west of Isfahan, central Iran, *Islamic Azad University, Mashhad Branch*, 4:75–84.

Nazari, M., Arian, M. A., Solgi, A., Zareisahamieh, R. and Yazdi, A. 2023. Geochemistry and tectonomagmatic environment of Eocene volcanic rocks in the southeastern region of Abhar, NW Iran, *Iranian Journal of Earth Sciences*, 15(4):228–247.
DOI: https://doi.org/10.30495/ijes.2023.1956689.1746

Nouri, F., Azizi, H., Stern, R. J. and Asahara, Y. 2023. The Sanandaj–Sirjan Zone (W. Iran) was a Jurassic passive continental margin: Evidence from igneous rocks of the Songhor area, *Lithos*, 440:107023.
DOI: https://doi.org/10.1016/j.lithos.2023.107023

Orihashi, Y., Nakai, S. I. and Hirata, T. 2008. U–Pb age determination for seven standard zircons using inductively coupled plasma–mass spectrometry coupled with frequency quintupled Nd–YAG ($\lambda = 213$ nm) laser ablation system: Comparison with LA–ICP–MS zircon

analyses with a NIST glass reference material, *Resource Geology*, 58:101–123.
DOI: https://doi.org/10.1111/j.1751-3928.2008.00052.x

Ousta, S. H., Ashja-Ardalan, A., Yazdi, A., Dabiri, R. and Arian, M. A. 2024. Petrogenesis and tectonic implications of Miocene dikes in the southeast of Bam (SE Iran): Constraints on the development of active continental margin, *Geopersia*, 14(1):89–111.
DOI: https://doi.org/10.22059/geope.2023.364334.648729

Pearce, J.A. and Stern, R.J., 2006. Origin of back-arc basin magmas: Trace element and isotope perspectives, *Back-Arc Spreading Systems: Geological, Biological, Chemical, and Physical Interactions*, 166:63–86.
DOI: https://doi.org/10.1029/166GM06

Pearce, J. A. and Norry, M. J. 1979. Petrogenetic implications of Ti, Zr, Y, and Nb variations in volcanic rocks, *Contributions to Mineralogy and Petrology*, 69:33–47.

Pearce, N. J., Perkins, W. T., Westgate, J. A., Gorton, M. P., Jackson, S. E., Neal, C. R. and Chenery, S. P. 1997. A compilation of new and published major and trace element data for NIST SRM 610 and NIST SRM 612 glass reference materials, *Geostandards Newsletter*, 21:115–144.
DOI: https://doi.org/10.1111/j.1751-908X.1997.tb00538.x

Peccerillo A., Taylor S. 1976. Rare earth elements in East Carpathian volcanic rocks. *Earth and Planetary Science Letters*, 32, pp. 121–126.
DOI: https://doi.org/10.1016/0012-821X(76)90050-9

Rapp R. P., Watson E. B. 1995. Dehydration melting of metabasalt at 8–32 kbar: implications for continental growth and crust-mantle recycling. *Journal of Petrology*, 36, pp. 891–931.
DOI: https://doi.org/10.1093/petrology/36.4.891

Rushmer T. 1991. Partial melting of two amphibolites: contrasting experimental results under fluid-absent conditions. *Contributions to Mineralogy and Petrology*, 107, pp. 41–59.

Salehpour S., Arian M. A., Rad A. J., Zarei Sahamieh R., Yazdi A. 2025. Geochemistry and technomagmatic environment of Eocene volcanic rocks in Yuzbashi Chay region, west of Qazvin (Iran). *Iranian Journal of Earth Sciences*, 17(1), pp. 1–13.
DOI: https://doi.org/10.57647/j.ijes.2025.1701.04

Shabanian N., Neubauer F. 2024. From Early Jurassic intracontinental subduction to Early–Middle Jurassic slab break-off magmatism during the Cimmerian orogeny in the Sanandaj–Sirjan Zone, Iran. *Journal of Asian Earth Sciences*, 106153.
DOI: https://doi.org/10.1016/j.jseaes.2024.106153

Shafaii Moghadam H., Li Q., Li X., Stern R. J., Levresse G., Santos J., Lopez Martinez M., Ducea M., Ghorbani G., Hassannezhad A. 2020. Neotethyan subduction ignited the Iran arc and backarc differently. *Journal of Geophysical Research: Solid Earth*, 125, e2019JB018460.
DOI: https://doi.org/10.1029/2019JB018460

Shakerardakani F., Neubauer F., Liu X., Dong Y., Monfaredi B., Li X.-H. 2021. New detrital zircon U–Pb insights on the palaeogeographic origin of the central Sanandaj–Sirjan zone, Iran. *Geological Magazine*, 158, pp. 2165–2186.
DOI: https://doi.org/10.1017/S0016756821000728

Shervais J. W. 1982. Ti–V plots and the petrogenesis of modern and ophiolitic lavas. *Earth and Planetary Science Letters*, 59, pp. 101–118.
DOI: https://doi.org/10.1016/0012-821X(82)90120-0

Smithies, R., Van Kranendonk, M. and Champion, D. 2007. The Mesoarchean emergence of modern-style subduction. *Gondwana Research*, 11, pp. 50–68.
DOI: https://doi.org/10.1016/j.gr.2006.02.001

Soltani Sisi, G. 2005. Geological map of Iran, 1:100000 series, sheet No. 5065. *Geological Survey and Mineral Exploration of Iran*.

Stacey, J.T. and Kramers, J. 1975. Approximation of terrestrial lead isotope evolution by a two-stage model. *Earth and Planetary Science Letters*, 26, pp. 207–221.
DOI: https://doi.org/10.1016/0012-821X(75)90088-6

Stern, R.J., 2010. The anatomy and ontogeny of modern intra-oceanic arc systems, *Geological Society, London, Special Publications*, 338:7–36.
DOI: https://doi.org/10.1144/SP338.2

Sun, S.-S. and McDonough, W.F. 1989. Chemical and isotopic systematics of oceanic basalts: implications for mantle composition and processes. *Geological Society, London, Special Publications*, 42, pp. 313–345.
DOI: https://doi.org/10.1144/GSL.SP.1989.042.01.19

Talebian Borojenie, H., Sheykhzakariaei, S.J., Dabiri, R. and Yazdi, A. 2025. Petrogenesis and tectonic implications of Neoproterozoic to Cenozoic A-type granitoids in NW Iran: geochemical and tectonic constraints. *Iranian Journal of Earth Sciences*, 17(4), pp. 1–19.
DOI: https://doi.org/10.57647/j.ijes.2025.16894

Tarney, J. and Weaver, B. 1987. Mineralogy, petrology and geochemistry of the Scourie dykes: petrogenesis and crystallization processes in dykes intruded at depth. *Geological Society, London, Special Publications*, 27, pp. 217–233.
DOI: https://doi.org/10.1144/gsl.sp.1987.027.01.19

Tavakoli, N., Davoudian, A.R., Shabanian, N., Azizi, H., Neubauer, F., Asahara, Y. and Bernroider, M. 2020. Zircon U-Pb dating, mineralogy and geochemical characteristics of the gabbro and gabbro-diorite bodies, Boein–Miandasht, western Iran. *International Geology Review*, 62, pp. 1658–1676.
DOI: https://doi.org/10.1080/00206814.2019.1583139

Tavakoli, N., Shabanian, N., Davoudian, A.R., Azizi, H., Neubauer, F., Asahara, Y., Bernroider, M. and Lee, J.K. 2021. A-type granite in the Boein-Miandasht Complex: Evidence for a Late Jurassic extensional regime in the Sanandaj-Sirjan Zone, western Iran. *Journal of Asian Earth Sciences*, 213, pp. 104771.
DOI: https://doi.org/10.1016/j.jseaes.2021.104771

Volpe, A.M., Macdougall, J.D., Lugmair, G.W., Hawkins, J.W. and Lonsdale, P., 1990. Fine-scale isotopic variation in Mariana Trough basalts: Evidence for heterogeneity and a recycled component in back-arc basin mantle, *Earth and Planetary Science Letters*, 100:251–264.
DOI: https://doi.org/10.1016/0012-821X(90)90188-4

Whitney, D.L. and Evans, B.W. 2010. Abbreviations for names of rock-forming minerals. *American Mineralogist*, 95, pp. 185–187.
DOI: https://doi.org/10.2138/am.2010.3371

Yazdi, A., Ashja-Ardalan, A., Emami, M.H., Dabiri, R. and Foudazi, M. 2017. Chemistry of minerals and geothermobarometry of volcanic rocks in the region located in southeast of Bam, Kerman Province. *Open Journal of Geology*, 7(11), pp. 1644–1653.
DOI: https://doi.org/10.4236/ojg.2017.711110

Zarasvandi, A., Rezaei, M., Raith, J., Lentz, D., Azimzadeh, A.-M. and Pourkaseb, H. 2015. Geochemistry and fluid characteristics of the Dalli porphyry Cu–Au deposit, Central Iran. *Journal of Asian Earth Sciences*, 111, pp. 175–191.
DOI: https://doi.org/10.1016/j.jseaes.2015.07.029